Root Niche Separation Can Explain Avoidance of Seasonal Drought Stress and Vulnerability of Overstory Trees to Extended Drought in a Mature Amazonian Forest

Valeriy Y. Ivanov[1,4]
Lucy R. Hutyra[2,3]
Steven C. Wofsy[2]
J. William Munger[2]
Scott R. Saleska[5]
Raimundo C. de Oliveira Jr.[6]
Plínio B. de Camargo[7]

[1]Department of Civil and Environmental Engineering, University of Michigan, U.S.A.
[2]Department of Earth and Planetary Sciences, Harvard University, U.S.A.
[3]Department of Geography and Environment, Boston University, U.S.A.
[4]Center for the Environment, Harvard University, U.S.A.
[5] Department of Ecology and Evolutionary Biology, University of Arizona, U.S.A.
[6]Brazil Agriculture Research Agency (EMBRAPA), Brazil
[7]University of São Paulo, Brazil

April 21, 2011
Submitted to the *Journal of Hydrology*

Valeriy Y. Ivanov (corresp. author), ivanov@umich.edu, (734) 763-5068; (734) 764-2275 (fax)
Lucy R. Hutyra, lrhutyra@bu.edu, (617) 353-5743; (617) 353-8399 (fax)
Steven C. Wofsy, swofsy@seas.harvard.edu, (617) 495-4566, (617) 495-4551 (fax)
J. William Munger, jwmunger@seas.harvard.edu, 617-495-5361, 617-495-2768 (fax)
Scott R. Saleska, saleska@email.arizona.edu, (520) 626-1500, (520) 621-9190 (fax)
Raimundo C. de Oliveira Jr., cosme@cpatu.embrapa.br, +55 (93) 3522-2203, +55 (91) 9991-9275
Plínio B. de Camargo, pcamargo@cena.usp.br, +55 (19) 3429-4068, +55 (19) 3429-4059 (fax)

Abstract

Large areas of Amazonian evergreen forests experience seasonal droughts extending for three or more months, and show maximum rates of photosynthesis and evapotranspiration during dry intervals. This apparent resilience is belied by disproportionate mortality of the large trees in manipulations that reduce wet season rainfall, occurring after 2-3 years of treatment. The goal of this study is to characterize the mechanisms that produce these contrasting ecosystem responses. A mechanistic vegetation-hydrology model is developed to test the roles of deep roots and of soil capillary flux to provide water to the forest during the dry season. Also examined is the importance of "root niche separation," in which roots of overstory trees extend to depth, where during the dry season they use water stored from wet season precipitation, while roots of understory trees are concentrated in shallow layers that access dry season precipitation directly. Observational data on canopy phenology, energy fluxes, soil moisture, and soil and root structure from the Tapajós National Forest, Brazil, provided comprehensive observational constraints on the model. Results strongly suggest that deep roots with root niche separation adaptations explain both the observed resilience during seasonal drought and the vulnerability of canopy-dominant trees to extended deficits of wet season rainfall. These mechanisms appear to provide an adaptive strategy that enhances productivity of the largest trees in the face of their disproportionate heat loads and water demand in the dry season. A sensitivity analysis exploring how wet season rainfall affects the stability of the rainforest system is presented. The model can be used to quantitatively predict ecosystem water balances and explore ecosystem tipping points under future climate change.

Index Terms: 1866, 1813, 1847, 1830

Keywords: water stress, drought avoidance, subsurface hydrology, ecohydrology, Amazon rainforest

1 Introduction

The role of the Amazon rainforests in the global cycles of carbon, water, and energy is well recognized and has been the subject of numerous studies (e.g., *Schlesinger*, 1997). Still, recent research indicates that some of the essential controlling factors of the rainforest function are yet to be fully understood. For example, of particular importance is the rainforest regulation of water dynamics since the vital climatic feature of the region is precipitation spatial and temporal variability (*Fitzjarrald et al.*, 2008). The pronounced rainy and dry seasons, particularly in the central and eastern Amazon Basin (e.g., *Sombroek*, 2001; *Malhi and Wright*, 2004), have a significant implication for the system function. Dry season is typically attributed to months with less than 100 mm total precipitation (e.g., *Shuttleworth*, 1988). Remote sensing (e.g., *Huete et al.*, 2006; *Myneni et al.*, 2007; *Saleska et al.*, 2007) and ground-based observations (e.g., *Saleska et al.*, 2003; *Goulden et al.*, 2004; *da Rocha et al.*, 2004; *Hutyra et al.*, 2007) indicate higher photosynthetic activity and increased CO_2 uptake and water fluxes during dry season than in the wet season. One logical inference is that the rainforest is at least in part light-limited, not water-limited, and thus enhanced radiation levels of dry seasons favorably affect forest productivity, resulting in higher transpiration fluxes (*Hutyra et al.*, 2007; *Nemani et al.*, 2003). Early modeling studies, however, often resulted in an opposite pattern of ecosystem dynamics. In a typical model simulation reproducing dry season conditions, available water was quickly depleted through evapotranspiration and/or recharge of deep aquifers, and water stress set in long before the end of drought conditions. Overall vegetation activity would be suppressed and model simulations thus did not permit the persistence of transpiration fluxes throughout the entire duration of the dry season (e.g., *Lee et al.*, 2005; *Saleska et al.*, 2003).

Various hypotheses have been proposed to explain the extremely high drought-tolerance of the rainforest, including 1) deeply penetrating root systems (*Nepstad et al.*, 1994; *Jipp et al.*, 1998; *Grant et al.*, 2009); 2) the phenomenon of "hydraulic redistribution" (e.g., *Oliveira et al.*, 2005; *Lee et al.*, 2005); 3) uptake of water directly by leaves during dry season rains and nighttime dew events (*Cardinot*, 2008); and, more recently, even the regional effect of high water table (*Fan and Miguez-Macho*, 2010). The existence and significance of deep roots has been underlined in several studies and there is evidence that deep rooting is an undeniably important factor in the ecosystem function (*Kleidon and Heimann*, 1999; *Schenk and Jackson*, 2002; *Ichii et al.*, 2007). The open questions are how deeply roots can really grow, what kind of hydraulic limitations exist on the transfer of water from deep locations to the top of canopy, and whether there are sufficient roots at deep locations. For example, *Nepstad et al.* (1994) estimated that only about 10% of the total rooting mass was at depths between 4 m and 10 m. However, in a modeling study, *Grant et al.* (2009) demonstrated that a root system to a depth of 8 m was needed to avoid water limitations for a five-month dry season. The phenomenon of hydraulic redistribution has been well documented for arid and temperate climate plant species (e.g., for a review see *Caldwell et al.*, 1998) and recently has been demonstrated for three species of trees in the Tapajós National Forest, Brazil (*Oliveira et al.*, 2005). Hydraulic redistribution is the process of water transfer by roots following the counter-gradient of soil water potential when transpiration uptake is negligible (*Oliveira et al.*, 2005; *Lee et al.*, 2005). Under this assumption, roots serve as passive hydraulic conduits. It should be noted that *Oliveira et al.* (2005) only indicated changes in the flow direction in roots, depending on day/night/season. The *Oliveira et al.* (2005) observations may not be a sufficiently strong argument to advocate the importance of

hydraulic redistribution on the entire ecosystem function, as was done by some studies (e.g., *Lee et al.*, 2005), since flow reversal does not immediately imply that significant moisture amounts can be transferred and deposited in soil surrounding roots (e.g., *Neumann et al.*, 2010). Furthermore, the most frequently cited *indirect* evidence of the phenomenon, such as the diurnal decrease-increase cycles of soil moisture observed by *da Rocha et al.* (2004), can be equally well attributed to the capillary action of clayey soils that dominate near their field site (e.g., *Silver et al.*, 2000). Other experiments near the site of *Oliveira et al.* (2005) even postulate that, in fact, the hydraulic redistribution mechanism cannot contribute significantly to the soil water dynamics (e.g., *Romero-Saltos et al.*, 2005). A recent claim of possibly predominant groundwater effects (*Fan and Miguez-Macho*, 2010) is not supported by field observations, e.g., there is no evidence of shallow water table for all flux tower sites in the Tapajós National Forest. Apparently, the question of the exact water-stress avoidance mechanism is far from being resolved. Other explanations should be attempted that will help focus future observational campaigns, so that "unfit hypotheses" (*Popper*, 1972) can be objectively evaluated.

This study makes further effort to address hydrology of an Amazonian rainforest. A vegetation-hydrology model that parameterizes the essential canopy-soil water-energy processes using a simplified three-big-leaf representation of canopy vertical structure is developed. The representation of very deep ($\sim$36 m) soil profile explicitly resolves the propagation of wetting and drying cycles into the soil column underlying forest vegetation. Comprehensive observational data from a flux tower site in Tapajós National Forest near km 67 of the Santarém-Cuiabá highway are used in this study. Meteorological data from the flux tower for the period of 2002 through 2005 serve as the model forcing. Observed canopy phenology,

energy fluxes, soil texture and water retention properties, and profiles of root biomass are used to parameterize and constrain the model performance. The study focuses on several possible explanations of the paradigm that either have not been considered in sufficient detail in numerical models or entirely not previously examined. Specifically, a set of numerical experiments has been designed to address: 1) the depth of rainforest root system as the only strategy for stress avoidance; 2) the capillary properties of clayey Oxisol soils that could possibly lead to the upward flow of water from soil layers below the deepest extent of roots; and 3) the existence of specific water uptake niches in the soil column, corresponding to root systems of trees located at different levels in the vertically structured canopy, i.e., overstory, mid-size, and understory trees.

An indirect evidence pointing to the latter hypothesis is the remarkable agreement of the main outcomes of two long-term rainfall exclusion experiments described in *Nepstad et al.* (2002, 2007) and *da Costa et al.* (2010) as well as a pan-tropical assessment of drought-related tree mortality by *Phillips et al.* (2010): in all studies large trees were consistently found to be the most vulnerable to prolonged droughts. For instance, *Nepstad et al.* (2002, 2007) described an experiment that simulated severe, four-year drought episode by excluding 60% of throughfall during each wet season for a 1-ha forest treatment plot located in Tapajós. The exclusion led to the propagation of the drought signal to deep soil layers resulting in 4.5-fold increased mortality rates among large trees and 2-fold among medium-size trees after four years of the experiment (*Nepstad et al.*, 2007). Strikingly similar findings have been reported for a rainfall exclusion experiment in the Caxiuanã National Forest by *da Costa et al.* (2010) and for permanent, monitored plots of the pan-Amazon RAINFOR project following the 2005 drought (*Phillips et al.*, 2010). A similar to *Nepstad et al.* (2002) scenario of exclusion of

wet season rainfall has been developed in numerical experiments of the presented study. The numerical experiments mimic the drying signal and severe water limitations experienced only by overstory trees in conditions of root niche separation. A subsequent sensitivity analysis has been carried out with respect to the key parameters of root water uptake that quantify plant water limitation. The results confirm that the existence of specific water uptake niches in the soil is the likeliest expression of a mechanism explaining plant water-stress avoidance and vulnerability of overstory trees to extended drought at the location of study site. They also point to the importance of wet season precipitation as the factor affecting the stability of the rainforest system. The observational data set, the overall design and methodology of numerical experiments, and the study inferences are presented in the following.

2 Data and methods

2.1 Site description

Data from the flux tower site in Tapajós National Forest (Brazil) (2^o51.4'S, 54^o57.5'W) near km 67 of the Santarém-Cuiabá highway BR-163 are used in the presented research. The site was a part of the Large-Scale Biosphere-Atmosphere Experiment in Amazonia (LBA-ECO) and has been used in a number of studies described in previous publications (e.g., *Hutyra et al.*, 2007; *Rice et al.*, 2004; *Vieira et al.*, 2004; *Saleska et al.*, 2003). It will be referred to as the "km 67" site throughout the rest of the manuscript. Additionally, a large throughfall exclusion experiment was established in the relative proximity of the flux tower ($\sim$5 km) in 2000 (*Nepstad et al.*, 2002), which monitored a variety of ecosystem characteristics in the 1-ha treatment and control plots (e.g., *Brando et al.*, 2008; *Nepstad et al.*, 2007). These

studies provide a complete description of different system characteristics and the reader is referred to the cited papers for details. The region has a mean annual temperature of 25^oC with a mean annual precipitation of $\sim$2,000 mm, varaible between 600 and 3,000 mm per year (*Nepstad et al.*, 2002). The area is subjected to a seasonal drought, i.e., months with less than 100 mm precipitation, with a mean span of 5 months, typically lasting from July 15 to December 15 (*Parrota et al.*, 1995). The water table is very deep, $\sim$100 m below the soil surface at a nearby location with similar topographic characteristics (*Nepstad et al.*, 2002). Soils are clay-rich, deeply weathered Oxisols. Patches of higher sand content (Santarém ultisols) occur on slopes and in topographic lows. The forest is located on flat terrain, an erosional remnant plateau, with a limited drainage network formed on sediments of the Barreiras formation (*Silver et al.*, 2000). The forest has a closed canopy with a mean height of approximately 40 to 45 m and emergent trees reaching up to 55 m. The vertical canopy distribution is stratified *Vieira et al.* (2004) with a fairly distinct three-level structure that represent the highest, mid-range, and smallest trees. The forest at the site exhibits a robust increase of latent heat flux during dry seasons (for details, see *Hutyra et al.*, 2007), responding to increased light levels (Figure 1a). The annual variation of foliage leaf area index (LAI) is within 10% of maximum value, with the maximum apparently out-of-phase with the radiation cycle (Figure 1b, *Brando et al.*, 2010). *Domingues et al.* (2005) showed that the leaf density was approximately constant throughout the canopy profile with about 35% of leaf area attributed to the top 10 m of the canopy.

2.2 Hydrometeorological forcing data

Gap-filled meteorological data for the period of 01/2002-01/2006 are used as atmospheric forcing to the model. Specifically, the hourly time series of the following variables observed at the flux tower at the km 67 site (*Hutyra et al.*, 2007) serve as the model input: hourly precipitation (measured at 42.6 m above the forest floor), air temperature (57.8 m), water vapor partial pressure (computed from vapor molar concentration measured at 62.2 m), wind speed (57.8 m), CO_2 partial pressure (measured as molar concentration at 62.2 m), atmospheric pressure (ground level), and incoming shortwave and longwave radiation fluxes (see also discussion below). Data gaps were insignificant for most of the variables and were filled with the mean monthly values corresponding to the hour of the day with missing value. Only radiation data contained a large fraction of gaps and thus several sources/methods were used to complete the series. The gaps in the time series of shortwave irradiance were filled using regressions with the series of observed photosynthetically active radiation (PAR). Two incomplete data sources on PAR were available for the km 67 site. The regression relationships constructed using these PAR series and global shortwave flux data explained much of the variability in observations: $r^2 = 0.966$ and 0.928, where r is the correlation coefficient.

In order to partition global shortwave radiation into direct beam and diffuse types as well as into visible (VIS) and near-infrared (NIR) spectral bands (which are the types of radiation forcing required by the model used in the study), a weather generator described in *Fatichi et al.* (2011) was used. Radiation data for clear sky and overcast conditions as well as data from Aerosol Robotic Network (AERONET, *Holben*, 1998) for Belterra Station (2^o51.5'S, 54^o57.5'W) on optical properties of the atmosphere were used to infer the parameters of

196 the atmospheric shortwave transfer module of the weather generator. For all-sky conditions,
197 approximate values of hourly cloudiness were computed. Cloudiness was subsequently used
198 to partition global radiation into the direct/diffuse types and VIS/NIR bands by the weather
199 generator.

200 Analysis of longwave radiation data observed at the km 67 site indicated their unreliability
201 and thus they were not used. Using data measured at the km 77 pasture flux tower site
202 (3^o1.2'S, 54^o53.3'W, *Sakai et al.*, 2004), a non-linear regression of longwave radiation flux
203 $L\downarrow$ with temperature T $[^oC]$ and vapor pressure e $[mb]$ was developed: $L\downarrow = \sigma(0.74 +$
204 $a\,e)(T + 273.15)$, where a was defined as 0.0068. Using data on T and e measured at the km
205 77 site, the series of longwave radiation data were derived and assumed to be representative
206 for the km 67 site. Small remaining data gaps were filled using the same regression equation
207 with temperature and vapor pressure observed at the km 67 site.

208 2.3 Soil hydraulic properties

209 The soils at the km 67 site study are clayey Oxisols that are deeply weathered with no
210 concretions or impeding layers, at least in the upper 12 m (*Nepstad et al.*, 2007). The
211 van Genuchten-Mualem soil hydraulic model (*van Genuchten*, 1980) was chosen to describe
212 the dependence of conductivity and soil matric pressure on moisture content. Due to the
213 absence of detailed, on-site measurements of soil hydraulic properties as well as uncertainty
214 associated with each indirect method, several approaches and data sources were used to
215 infer the saturated conductivity and soil water retention parameters. Previously reported
216 soil water retention parameters by *Belk et al.* (2007) did not favorably compare with the
217 other independently obtained parameterizations (see sections 2.3.2 - 2.3.4 and Figure 2) and

therefore were not used. Note that the generated ensemble of soil parameterizations permits addressing robustness of study inferences with respect to uncertain properties of the soil. The following describes methodology used in obtaining the parameter values.

2.3.1 Saturated hydraulic conductivity

Values of the saturated hydraulic conductivity were digitized from the manuscript of *Belk et al.* (2007), who measured conductivity over the 4 m soil depth. Geometric averaging of depth-interpolated values was carried out to obtain $K_{sn} = 35.6$ $[mm\ hour^{-1}]$ for the 0.05-0.3 m depth range and $K_{sn} = 14.1$ $[mm\ hour^{-1}]$ for the 0.3-4.0 m depth range. These values were used in the two scenarios described in sections 2.3.2 and 2.3.3.

2.3.2 Measured soil water retention data

The data were obtained from R.-C. de Oliveira, Jr. (Brazilian Agricultural Research Corporation *EMBRAPA Amazonia Oriental*) in 2007. Soil samples were collected at a location that is in a relative proximity of the km 67 flux tower site, however the exact location was not recorded. Laboratory measurements of water retention properties were carried out for the following soil matric pressures: 6, 10, 33, 100, and 1500 kPa. Samples were taken from the following depths: 5, 15, 30, 50, 100, and 200 cm. Due to significant differences in the soil water retention data between the surface layer and deeper locations, the measurements were grouped according to the following depth ranges: 0.05-0.3 $[m]$ (what is referred to as "CO - surface" group) and 0.5-2 m ("CO - deep" group). A non-linear optimization of parameter values of the *van Genuchten* (1980) model was subsequently carried out. The data and the fitted water retention curves for the two depth ranges are shown in Figure 2. The corresponding parameter values are provided in Table 2.

2.3.3 Parameter estimation using pedotransfer functions

Tomasella et al. (2000) developed generic pedotransfer functions for South American soils allowing one to derive the parameter values of the *van Genuchten* (1980) model based on soil textural and chemical composition. Field soil texture data were obtained by the authors in 2003 (unpublished data set): the surface soil composition was reported as 91% clay, 7.8% silt, and 1.2% sand. The organic carbon content was reported as 2.68 [$g\ kg^{-1}$] and soil bulk density was measured as 1.0225 [$g\ cm^{-3}$]. As fractions of fine sand and coarse sand were unknown, they were assumed to be either 0, 50, or 100%. Using the *Tomasella et al.* (2000) functions, three parameter sets were estimated assuming these fractions. The obtained parameter sets differed only slightly and thus they were geometrically averaged in order to obtain a single parameter set. The derived water retention curve representative of the entire soil column is shown in Figure 2 (the "Tomasella et al. (2000)" curve). The corresponding parameter values are provided in Table 2 as the "TH" parameterization.

2.3.4 Inverse parameter estimation

An inverse method of *Hou and Rubin* (2005) was used to derive soil properties using soil water dynamics data resolved at multiple depths. The only available high-frequency, long-term record of soil moisture data was available for a site at km 83 of the Santarém-Cuiabá highway (*Bruno et al.*, 2006). This data set was used in the inverse estimation procedure. Eight cases were selected corresponding to 10-11 hour night-time intervals with zero or insignificant observed evaporation. The cases included periods with the highest and lowest observed soil moisture, as well as the cases with the highest moisture variability in the 10 m soil profile. The derived water retention curve representative of the entire soil column is

shown in Figure 2. The depth-uniform saturated hydraulic conductivity was estimated to be $K_{sn} = 26.9$ $[mm\ hour^{-1}]$. The corresponding parameter values are provided in Table 2 as the "MRE" parameterization.

2.4 Root profiles

Data on the distributions of root biomass density were obtained as one of the outcomes of the throughfall exclusion experiment (*Nepstad et al.*, 2002) that was carried out in the relative proximity of the flux tower ($\sim$5 km). For the treatment site, only data obtained before the beginning of the experiment were used. Observations of fine root biomass were used (a fine root has the diameter smaller than 2 mm). Suberized fraction of a fine root is small and almost the entire root surface can be used for plant moisture uptake (*Taiz and Zeiger*, 2006, p. 56). Fine root distributions were therefore associated with uptake profiles; they were used in the modeling efforts (section 2.5.4).

The original raw data (obtained from D. Ray, the University of Maine, School of Forest Resources) were transformed to obtain biomass density distributions with depth. As Figure 3a clearly shows, there is a generally good agreement in terms of shapes and absolute magnitudes among several profiles obtained in the study of *Nepstad et al.* (2002) at different times and locations. The important features are a) the high concentration of most fine roots in the surface 0-1 m layer and b) the fairly slowly decaying biomass density in the 3-6 m soil layer. A "generalized" root profile was created based on the actual measurement data shown in Figure 3a. The profile was computed as the average of all available profiles in the 0-3 m depth range and as a linear approximation of the root biomass decay in the 3-6 m depth range. Note that the biomass density over the latter soil layer is small but not entirely

negligible: when integrated, it represents ∼12% of the total root mass if one assumes that there are no roots beyond the maximum observational depth $Z_{RootS} = 6\ m$. The latter assumption is however fairly extreme and unrealistic, given previous observational evidence on root depths in the Amazon (e.g., *Nepstad et al.*, 1994). Consequently, this study has attempted to construct an additional scenario that would provide a second "envelope" on the feasible range of root distributions with depth. Specifically, the linear profile of the root biomass in the 3-6 m soil interval was extrapolated to its zero intercept with the depth axis and the depth corresponding to 95% of the total root biomass content was identifed. This depth was equal to $Z_{RootD} = 30.2\ m$ and thus was assumed to be the maximum root depth. The root density profile terminates at this depth and the profile in the range of [3, Z_{RootD}] m is estimated to contain ∼41% of the total root mass.

Observations of dead fine root biomass were also available from *Nepstad et al.* (2002). It was inferred that their relative density distributions (absolute density divided by the total root mass) were entirely identical to that of live fine roots (not shown). While being indirect, this evidence provides an additional confirmation of the chosen strategy in defining the feasible range of maximum plant root depths Z_{RootS} and Z_{RootD}.

2.5 Modeling efforts

An ecohydrological model that parameterizes essential canopy-soil water-energy processes using a three-big-leaf representation of canopy vertical structure and a finely resolved deep soil profile was developed in this study. As is the case with any modeling effort, a number of simplifying assumptions were made in the representation of structural elements of vegetation-hydrology system, its intra- and inter-annual dynamics, as well as in the description of

relevant physical processes. These are outlined in the following.

2.5.1 Ecohydrological model

A model of vegetation-hydrology interactions (*Ivanov et al.*, 2008), tRIBS+VEGGIE, is used in this study. The model mimics principal water and energy processes over the complex topography of a river basin and links them to essential plant biochemical processes and phenology. The model design emphasizes dynamic interactions between vegetation system and subsurface hydrological dynamics. Each computational element exhibits a "big-leaf" representation of canopy coupled to a multi-layer soil-root model that computes soil moisture and heat transport, and root water uptake.

In this study, however, the model was applied at the plot scale and vegetation dynamics were not explicitly simulated. Only the biochemical model of canopy stomatal behavior (*Farquhar et al.*, 1980; *Collatz et al.*, 1991) was used to simulate the response of latent heat flux to the ambient environment. The amount of leaf area as well as structural characteristics of vegetation were imposed as pre-determined model input (see section 2.5.3). Furthermore, the model formulation described in *Ivanov et al.* (2008) has been substantially modified to adapt the model to conditions of the study site that exhibits complex canopy structure and deep soils. These changes are briefly outlined in Appendix A and B. For a reader's convenience, Appendix C provides the formulation of a heuristic soil moisture availability factor, β_T [−], which is frequently used throughout the text. The factor β_T is used to regulate stomatal conductance and its departure from unity indicates soil control on transpiration flux and water limitation experienced by vegetation. Table 3 contains the parameter values used in this study. The notation used for the parameters is the same as that of *Ivanov et al.* (2008).

2.5.2 Soil profile

In representing soil profile in the model, two conditions had to be accounted for: a) the capability to incorporate the deepest root profile with $Z_{RootD} = 30.2\ m$; and b) the need of providing a sufficient soil buffer under the root zone to alleviate the effect of assumed free drainage boundary condition at the bottom of the soil column. With respect to the latter, the intention was to create a soil buffer that could generate upward unsaturated flow were sufficiently high tensions developed in the root zone because of moisture uptake by roots. Consequently, a deep, 36 m soil profile was used to model the subsurface soil moisture dynamics. A regular mesh resolution was selected to be 30 mm, which therefore led to 1,200 computational nodes in the subsurface domain.

2.5.3 Above-ground vegetation components

A three-big-leaf representation of the forest canopy was developed in an attempt to represent the vertical structure of the canopy, which has been observed to be distinctly stratified (*Vieira et al.*, 2004). *Rice et al.* (2004) describe "emergent", "canopy", "subcanopy", and "suppressed" trees. Translating this naming style to the terminology used in this study: the "top-canopy" (overstory) trees were assumed to represent the "emergent" and "canopy" trees; the "mid-canopy" and "bottom-canopy" (understory) trees were assumed to represent "subcanopy" and "suppressed" trees, respectively. These types of trees were assumed to be sufficiently different in their biophysical and biochemical properties, for example, reflecting observed changes in characteristics of sunlit and shaded plants (e.g., *Taiz and Zeiger*, 2006). The outcome of such an assumption is that different canopy levels were effectively represented to correspond to different "plant functional types", even though some of the same species

are likely to be present in each canopy level. Note the interchangeable use of "tree type", "plant type", and "canopy layer" in the following text. Details of treatment of canopy layers are presented in Appendix A; the corresponding parameter values are provided in Table 3.

The amount of leaf area as well as structural characteristics of vegetation were imposed as pre-determined model input. The data on canopy dynamics were obtained from the database of the Large Scale Biosphere-Atmosphere Experiment in Amazonia (LBA) (*http://lba.cptec.inpe.br*). This dataset contains measurements of total leaf area index (LAI) obtained at monthly intervals in the control plots of the rainfall exclusion experiment (*Nepstad et al.*, 2002). The LAI data span the period of 2000 through 2004. According to *Domingues et al.* (2005), the leaf density is approximately constant throughout the canopy profile at the site; consequently, the mean annual cycle of LAI for each of the "big leaves" was obtained by dividing the total LAI (shown Figure 1b) by three.

The amount of stem area was assumed to be 0.2 $[m^2\, m^{-2}\, ground area]$ for each of the tree types. Each canopy layer was assumed to be uniformly occupying the entire plot area, i.e., the vegetation fraction was set to one for each of the plant types. This apparent simplification neglects the spatial heterogeneity of canopy, i.e., the existence of gaps as well as patches with LAI higher than the one assumed. Remote-sensing data that permit the inverse estimation of LAI, e.g., the data from Moderate Resolution Imaging Spectroradiometer, MODIS (*http:modis.gsfc.nasa.gov, Myneni et al., 2002)*, do not offer sufficient resolution and quality to assess the degree of such variability at the study site. The importance of representation of canopy heterogeneity at the tree scale is hard to assess since relevant studies are still in their nascence (e.g., *Bohrer et al.*, 2009).

2.5.4 Below-ground vegetation components

Each of the tree types defined above according to the canopy level (section 2.5.3) contributes to the distribution of fine root biomass described in section 2.4. A first-order assumption one can make is that each of the types contributes equally to the observed density at any depth z and therefore root density for any tree type can be obtained as the total root biomass divided by three. For each of the considered maximum root depths, Z_{RootD} and Z_{RootS}, this serves as the "control" scenario (Figure 3b) against which all other root distribution scenarios are compared.

Certainly, the control root distribution case is only one plausible scenario of the shape of individual profiles corresponding to trees that have different positions in the canopy. Since it is practically impossible to quantify the distribution of a root fraction of a given tree type in the bulk root biomass from *in situ* observations and, to the author's knowledge, there are no available generic methodologies, this study has generated an ensemble of individual root distributions using the following qualitative constraints: 1) the top-canopy (overstory) trees have deeper roots and their root fraction at shallower soil depths should be smaller than that of trees located lower in the canopy; 2) the bottom-canopy (understory) trees have shallower roots and their root fraction at shallower soil depths should be larger than that of trees located higher in the canopy; 3) the roots of mid-canopy trees have a somewhat intermediate position and fraction as compared to the roots of top- and bottom-canopy trees; 4) the distribution of the total root biomass obtained as the sum of individual profiles at each depth has to be equal to the generalized profile described in section 2.4. The developed ad-hoc partition procedure yielded twelve additional permutations of individual root profiles that are illustrated in Figure 3b. As the number of permutation scenario increases, the

396 profiles become more different from the "control" root scenario and trees of the upper canopy
397 level contain progressively higher fraction of roots at deeper locations (Figure 4b, left hand-
398 side dashed line), while trees of the bottom canopy layer contain higher fraction of roots
399 at shallower soil layers (Figure 4b, right hand-side solid line). For example, in the case of
400 largest difference among the profiles, the roots of understory trees extend only to $\sim$1.2 m,
401 the root depth of mid-canopy trees is $\sim$2.8 m, while roots of overstory trees occupy the entire
402 depth Z_{RootD}.

403 The depth $Z_{RootS} = 6$ m was considered in the design to represent another choice of the
404 maximum possible root depth. Thirteen root permutations were generated by terminating
405 the individual profiles shown in Figure 3b at the depth Z_{RootS} to exclude roots beyond that
406 depth.

407 The ecohydrology model requires the input of a potential strength of moisture sink in
408 each subsurface mesh node (*Ivanov et al.*, 2008). Such a profile is obtained by computing the
409 fraction of roots contained in a control volume of each mesh node with respect to the total
410 root biomass. Twenty six permutations of fractional profiles for the two cases of maximum
411 root depth are illustrated in Figure 4.

412 2.5.5 Soil moisture initialization

413 The deep soil profile of a fine-textured soil may exhibit significant memory effects due to
414 the persistence of soil moisture initial conditions in simulations. This study attempted to
415 minimize such adverse initialization impacts by using a model "spin-up." Specifically, each
416 scenario of maximum root depth (Z_{Root}) for each soil type was simulated with 20 years of
417 meteorological forcing obtained as five four-year cycles of the original forcing data, 01/2002-
418 01/2006. The soil matric head profile at the end of each of these spin-up simulations was

used to initialize simulations for the corresponding combination of soil type and root depth.

3 Results

3.1 Model calibration

The tRIBS+VEGGIE model does not have an automated parameter calibration routine. Manual model calibration was carried out with the main objective to match the observed daily and seasonal cycles of net radiation, latent and sensible heat fluxes.

Since the study addresses the effects of dry periods on vegetation water uptake, the soil hydraulic parameters (Table 2) and the root fractions specifying the strength of transpiration moisture sinks (see Appendix C, equation (C-2)) should also be considered as unknown parameters. An arbitrary choice of soil type and root distribution would be unjustified since both can strongly affect the dynamics of plant water limitations. Therefore, the calibration strategy was based on the assumption that forest *does not* experience any water stress during drought periods. An empirical evidence of an increase of forest greenness during prolonged dry periods (e.g., *Huete et al.*, 2006; *Myneni et al.*, 2007; *Saleska et al.*, 2007) support such an assumption to a certain extent. During calibration, water stress for each tree type was artificially set to zero at each computational step and, consequently, calibration was soil-type and root-distribution independent. As a result, latent heat flux, simulated accounting for the energy constraints of (B-5) - (B-7) (Appendix B), essentially represented "potential evapotranspiration."

Note that the total observed day-time sensible and latent heat fluxes are lower than the observed net radiation: by 21.5% during wet season and by 19.5% during dry season periods

(see a detailed discussion in *Hutyra et al.*, 2007). This substantially complicates the definition of an exact energy partition. Since net radiation was believed to be measured more precisely than heat fluxes, its accurate simulation at the daily and seasonal scales was specifically targeted. The simulated net radiation thus matched observations nearly perfectly, as will be demonstrated in section 3.4.

By design, the model conserves energy and therefore any partition of simulated net radiation into heat fluxes cannot compare favorably with the measured values because of the aforementioned 19.5-21.5% heat imbalance in observational data. This "surplus" heat energy was distributed among the fluxes of latent, sensible, and ground heat and fluxes going into storage (heat exchanged by precipitation was not accounted for, see *Hutyra et al.*, 2007, for further statement of issues related to seasonal heat budget closure). To some extent, the final outcome of calibration is therefore affected by this subjective partition; but it is difficult to assess its exact impact. Several additional simulations were carried out in which parameters were re-defined, so as to make either latent or sensible heat receive a higher fraction of the "surplus" energy (not shown). It was inferred that the main conclusions of this study hold regardless of the decision made in calibration.

All of the model parameters used in the description of energy fluxes are provided in Table 3. Among these, the parameters of the "Interception" and "Water uptake" groups were not modified. Most of the "Biophysical" parameters were assigned based on values reported in literature (e.g., *Bonan*, 2008); only α_{Λ}^{leaf} and τ_{Λ}^{leaf} (VIS band) were slightly modified to represent the properties of vegetation acclimation to different vertical positions in the canopy. Using the same considerations, only $V_{max\,25}$ and $\epsilon_{3,4}$ parameters were calibrated in the "Biophysical" group.

Because of the long-term integration scale, the calibrated diurnal heat flux cycles for wet or dry seasons do not exhibit significant differences with respect to the cycles obtained for many combinations of soil type and root distribution. The discussion of diurnal energy cycles will thus be presented later in section 3.4, based on Figure 8. The annual cycle of evapotranspiration obtained in the calibration procedure is illustrated in Figure 5a, as the "no stress" scenario. As seen, its comparison with the annual cycle derived from the observational data is qualitatively satisfactory.

3.2 Annual cycle of evapotranspiration and water stress: identical root distributions

Figure 5 presents the simulation results as averaged annual cycles of evapotranspiration components computed for the three soil scenarios under the assumption of the *identical* root fractional distribution (i.e., the "control" distribution, see section 2.5.4 and Figure 3b). Specifically, the maximum root depth was set to either Z_{RootD} or Z_{RootS} and all tree types were assigned to have the identical root profile, which is the root scenario #1 (see Figure 3b). Figure 5a illustrates that the model exhibits poor performance during dry seasons, i.e., a depressed flux of total evapotranspiration is simulated, as compared to observations (particularly, for the Z_{RootS} scenarios). As Figure 5a and 5b show, evaporation from soil and canopy interception storage show no sensitivity to any of the soil or root scenarios. The poor model performance during the period of August through December is thus because of dampening of the transpiration flux as the dry season progresses. The case of shallower root system (i.e., the maximum depth is $Z_{RootS} = 6\ m$) exhibits highest sensitivity for all soil types.

Figure 5c illustrates the cycles of the soil moisture availability factor (see Appendix C), β_T, computed as the average for the three tree types. The departure of β_T from unity indicates soil control on the transpiration flux and water limitation experienced by vegetation, i.e., $(1 - \beta_T)$ can be interpreted as a metric of water stress. As seen in the figure, all of the soil-root scenarios resulted in some degree of water stress experienced during dry periods. However, the average stress is fairly small for the $Z_{RootD} = 30.2\ m$ root scenario. The latter result implies that having (very) deep roots may be a sufficient strategy for avoiding the drought stress (the annual root water uptake is distributed over a larger soil depth, which makes the uptake density smaller per unit depth).

3.3 Sensitivity of evapotranspiration to niches of water uptake: vertically varying root profiles

Following the simulations that assumed the identical root distribution for trees having different positions in the canopy, vertically varying root profiles (corresponding to specific uptake niches discussed in section 2.5.4) were introduced. In addition to the "control" root profile, 12 permutations of individual root profiles were used for the two maximum root depths, Z_{RootD} and Z_{RootS}, resulting in 26 root scenarios for each soil type and, therefore, 78 total simulation scenarios. Figure 6a illustrates the factor β_T computed as the time-average value for a particular permutation scenario of root distribution (also averaged across the tree types). As seen, the more vertically "segregated" the profiles become (i.e., the higher the root scenario number), the less overall stress is reproduced by the model. The shallower root scenarios exhibit substantially higher sensitivity to root permutations than deeper root scenarios.

Figure 6b shows the pattern of the root mean square error ($RMSE_{ET}$) of mean daily evapotranspiration with respect to the observed magnitudes. The behavior does not replicate that of β_T but this can be explained by the fact that, overall, the model overestimates evapotranspiration flux. The higher β_T implies even higher magnitudes, which thus lead to a somewhat poorer comparison of the simulation results in terms of $RMSE_{ET}$ for larger numbers of root scenario.

Figures 6c and 6d interpret the patterns of β_T and $RMSE_{ET}$ behavior with respect to the root scenarios in terms of times series of evapotranspiration flux. The "TH" soil type is used that exhibited the highest water stress for the "control" root profile (Figure 5c) as well as the highest sensitivity of results to the permutations of tree root profiles (Figure 6a). As the root scenario number increases, indicating the growing degree of difference in the root fractional distributions, the model performance improves during dry seasons. This is particularly pronounced for the the shallower root scenarios that correspond to the maximum root depth Z_{RootS} (Figure 6d). The effect of improvement is not as pronounced for the dry season of month 20 through 26; a closer inspection however points to a possible problem in radiation forcing of the model for this time period.

One has to keep in mind that as the center of mass of root fractional distribution changes with the number of permutation scenario, so does the inter-related effect of moisture uptake because of the continuity of soil water profile. In other words, trees taking up moisture in a particular region of the soil profile necessarily impact uptake characteristics in other soil layers. So, how are the scenarios exhibiting less water stress expressed in terms of the subsurface moisture dynamics? Figure 7 illustrates the temporal evolution of soil moisture profile for the two root scenarios corresponding to the maximum root depth Z_{RootS}: the

identical, "control" root scenario (#1) and scenario #13 (assumes that overstory trees have an almost uniform profile and thus the center of mass of root density is at a deeper location, while trees of the bottom canopy layer contain all roots within the top 1.2 m). The figure clearly shows that the root scenario #13 avoids the extreme seasonal drying of the upper soil layer, where the "control" root scenario assumes the location of the centers of root mass for all trees. The scenario #13 leads to a more uniform distribution of the drying signal with depth. It can be generally inferred that the variance of soil moisture profile over the root zone depth during dry seasons is smaller for the higher root scenario number (not shown). It can also be concluded that there is no significant effect of root distribution on the soil moisture dynamics during wet periods, except for the year of 2003 that had an unusually low wet season rainfall. By wetting the deep soil profile down to 36 m (not shown), wet season precipitation appears to have a "re-setting" effect on soil water as the next drying season starts at an almost uniform profile of moisture near 0.55-0.57 volumetric content. As argued later, this is an important characteristic of soil moisture seasonality that might affect stability of the rainforest system from the perspective of soil water limitation on photosynthesis. Note that while related, this is different from the analysis of *Hutyra et al.* (2005) who used drought frequency as a surrogate metric of the vulnerability and resilience of Amazonian vegetation (see a discussion in section 4.2).

3.4 Seasonality of energy fluxes

Figure 8 illustrates the observed and simulated diurnal cycles of energy fluxes. The results correspond to the "CO" soil parameterization, root scenario #6 that did not exhibit appreciable water stress and thus the results are also representative of calibration (see section

552 3.1).

553 The observed cycle of net radiation is almost perfectly reproduced in the simulation
554 results; however, the simulated heat cycles exhibit certain differences from observations. As
555 pointed out in section 3.1, one of the principal difficulties in objective evaluation of such a
556 comparison is the fact that measurements of latent and sensible heat fluxes do not balance
557 the observed net radiation by about 20%. Since the modeled fluxes have to conserve net
558 radiation exactly, the difference with observations was subjectively distributed among the
559 different flux terms. The inclusion of ground heat (small) and storage (Appendix A) terms
560 helps in balancing the net radiative flux but the overall partition does not *appear* to be most
561 appropriate. For example, sensible heat flux is generally "overestimated" throughout the day;
562 the latent heat flux is "underestimated" in the first half of the day but is "overestimated"
563 during the second half. The underestimation effect is partially due to the inclusion of the
564 heat storage term; yet, the net effect is that the total evapotranspiration is somewhat larger
565 than observed, particularly during dry seasons (see Figure 5a).

566 Figure 9 shows the computed temperatures of canopy layers and undercanopy ground
567 (subplots (a) and (b)) that lead to the modeled energy partition. The figure also illustrates
568 the partition of the total simulated latent heat flux into contributions from different canopy
569 layers (subplots (c) and (d)). The results are consistent: the top canopy layer exhibits
570 highest temperatures during the day-light hours and the lowest temperatures during night-
571 time hours; middle and bottom canopy layers show progressively smaller diurnal temperature
572 variability and are somewhat warmer than the above-canopy air temperature throughout
573 the day; ground surface temperature has the lowest diurnal variability and exhibits cooler
574 temperatures during day-light hours because of low levels of radiation reaching the forest

floor. The partition of the total canopy layer latent heat shows a peculiar feature of the system: despite the assumed same LAI for all canopy layers, the top canopy level contributes by far the highest evapotranspiration flux, with lower canopy levels contributing progressively smaller fluxes. Such a feature is apparently related to the substantially higher light levels that are simulated for the top canopy, and, to a lesser extent, to the assigned distribution of V_{max} values (Table 3). The implication of this result is that the influence of soil or root distribution on the total forest evapotranspiration is conveyed through the effect on the function of overstory trees. Note also that by harvesting most radiation and transpiring the largest amounts of water, the overstory trees should be most vulnerable to fluctuating rainfall. However, as inferred and argued later, this has led to a specific adaptation strategy in terms of their root distribution.

3.5 Soil's effects

Three soil types were used in the study and the relevant question one has to ask is whether soil hydraulic properties exert a significant effect on the simulated dynamics of evapotranspiration and how they might be related to the root vertical variability. One may hypothesize, for example, that the "optimal" root distribution would minimize water losses from the root zone. The results shown in Figure 10 partially confirm such an assumption. Specifically, Figure 10 shows the cumulative net flux at the bottom of root zone of each tree type obtained for the entire simulation period (positive values indicate downward flux recharging deeper aquifers). As the root scenario number increases, the net flux from the root zone of overstory trees exhibits a minimum for scenarios #6 - 8 for the deeper root scenarios (subplots (a) through (c)); and progressively decreases for the shallower root scenarios (sub-

plots (d) through (f)). The losses from the root zones of understory trees and mid-canopy trees progressively increase for the deeper root scenarios; in the case of the shallower root scenarios, they reach a minimum for the scenarios #8 - 11. Note also that the results are only marginally sensitive with respect to the soil type: all types lead to essentially the same magnitudes of the net flux.

Another plausible effect hypothesized at the beginning of this study is that soil's capillary properties may impact moisture availability in the root zone. Specifically, if a sufficiently high gradient of soil matric potential is created in the root zone because of moisture uptake by plants, a flow in the direction opposite to the gravitational force may take place. Roots may thus start "pulling" water from soil layers below the root zone, thereby generating an additional moisture source. The predominance of fine texture clayey soils at the site makes such a hypothesis theoretically possible.

Figure 11 illustrates the cumulative upward flux into the root zone of each tree type obtained for the entire simulation period. Only results for the shallower root scenarios are shown as the fluxes were zero for all soil-root combinations in the case of scenarios corresponding to the maximum root depth Z_{RootD}. The total upward flux is very small for all considered cases and represents smaller than one hundredth of percent of the total annual transpiration by trees at all levels. The results are consistent among all soil types. The conclusion therefore is that capillary flow into the root zone from deeper layers cannot represent a significant surplus of water available for transpiration uptake.

Note that simulated subsurface water dynamics may exhibit minor diurnal fluctuations of near-surface soil moisture (not shown). They are related to the capillary effects of periodically developing high gradients of soil water potential during dry periods. Specifically, moisture

decreases during day-time because of transpiration and increases at night-time because of the capillary pull of water from lower depths. These dynamics can only be observed in shallow soil layers (e.g., see Figure 3 in *da Rocha et al.*, 2004). They dissipate with depth and become insignificant at the bottom of root zone of any tree type represented by the model (e.g., Figure 11). Note that they are only related to the soil's effect and have nothing to do with the effect of hydraulic redistribution hypothesized earlier by a number of studies with respect to empirically obtained soil moisture data at the km 83 flux tower site *da Rocha et al.* (2004).

4 Discussion

4.1 Root niche separation as the likeliest expression of adaptation strategy

One cannot completely resolve the exact water-stress avoidance mechanism without additional information. Given the amount of water evaporated in the dry season, it is clear that roots must extend to several meters. The notable result that largest trees die first when there is a wet season rainfall deficit, but only after several years, suggest that the largest trees are very deeply rooted. It also indicates that trees allocate roots so that trees occupying particular niches in the canopy have roots in comparable niches in the soil profile. In the long-term rainfall exclusion experiment in Tapajós, detailed in *Nepstad et al.* (2007), a severe, four-year drought episode that was simulated by excluding 60% of throughfall during each wet season for a 1-ha forest treatment plot. After 3.2 years of the experiment, "*surprisingly, the mortality of large trees began only during the final year of the experiment...*

641 *the treatment resulted in ... mortality rates increased 4.5-fold among large trees (> 30 cm*
642 *dbh) and twofold among medium trees (10-30 cm dbh) ... whereas the smallest stems were*
643 *less responsive*" (*Nepstad et al.*, 2007). The following discussion draws an important analogy
644 between the outcomes of this field monitoring program and inferences of this study.

645 *A priori*, if a decrease of wet season precipitation is imposed in numerical simulations, a
646 similar effect of vulnerability of overstory trees should emerge, provided the model realisti-
647 cally reproduces relevant processes of heat-water exchange. Obviously, the effect can only be
648 expressed in terms of increased water stress, not mortality, as the latter cannot be reliably
649 modeled in a deterministic fashion. In an attempt to verify this notion, a rainfall scenario
650 was developed in which precipitation was reduced by 60% from January through June of each
651 year, over the period of 01/2002-01/2006, i.e., thereby mimicking the design of *Nepstad et al.*
652 (2002), who carried out their monitoring in the close proximity to the km 67 site. Figure
653 12 illustrates a comparison of dynamics of the soil moisture availability factor β_T obtained
654 in simulations with observed and reduced wet season precipitation. The identical, "control"
655 root scenario #1 and the root scenario #13 (highest differences among the root profiles cor-
656 rresponding to trees at different canopy levels) were used. In simulations described in section
657 3.3, the root scenario #1 exhibited maximum, while scenario #13 exhibited minimum water
658 stress, the stress being interpreted as $1 - \beta_T$. As seen in the figure, the scenario #13 with
659 observed (not decreased) precipitation forcing exhibits only minor water deficiencies during
660 three dry seasons and they are only characteristic of understory trees. Overstory trees are
661 not water-limited and this is the case for both soil types, as inferred from Figures 12a and
662 12b.

663 For the identical root scenario #1, the 60% decrease of wet season precipitation leads to

similar water stresses experienced by *all* trees (Figures 12a and 12b, blue lines). This would imply nearly identical mortality rates for overstory and understory trees. One can infer that deep roots, without root niches, is likely to produce more uniform mortality than observed.

For the root scenario #13, the 60% decrease of wet season precipitation does *not* affect water availability of understory and mid-canopy trees significantly: they are able to transpire taking up most of the dry season and a fraction of wet season precipitation. Similarly, the effect of precipitation shortage is not appreciable for overstory trees until 2 - 2.5 years after the beginning of simulations. This implies that top-canopy trees exploit water surplus stored in deep soils recharged via earlier wet season rainfall. The water stress sets in towards the end of the second dry season and aggravates severely by the end of the fourth year. At that time, overstory trees cannot satisfy their water needs by more than 50% (Figures 12a and 12b). In actual conditions, this would translate in an increase of mortality of overstory trees. To provide a better insight, Figure 13 provides a graphical illustration of the soil water simulations, when the root permutation scenario #13 is assumed. It shows the depletion of deeper soil moisture reservoir during the first 2-2.5 years. A subsequent aggravation of conditions for depths larger than 3.5 m is apparent, as wetting fronts resulting from rainfall events do not penetrate beyond that depth.

The above results demonstrate that differential rooting depths can explain both the avoidance of seasonal drought stress by the entire rain forest ecosystem and vulnerability of overstory trees in conditions of a long-term drought. This strongly indicates that root niche separation is the likeliest expression of the evolutionary adaptation strategy resulting from a trade-off between the requirement of sustained productivity for canopy-dominant trees and the risk of periodic soil water limitation.

4.2 Wet season rainfall as key factor of ecosystem stability

Qualitatively comparing Figure 13 with Figure 7, one may propose that by wetting the deep soil profile (down to 36 m, not shown), wet season precipitation has a "re-setting" effect on soil water, so that plants transit to dry season conditions with plentiful moisture. Because overstory trees can access deeper soil layers, moisture that takes its origin from wet season rainfall may exert a buffering effect on severity of drought conditions of any particular year (or two, as the simulations demonstrate). However, if dry conditions persist for a period of time longer than the duration of the buffering effect, overstory trees will reach a "tipping" point in water stress and a sharply growing mortality would be the outcome. Mid-canopy and understory trees will likely also become vulnerable to drought conditions once the overstory canopy becomes thinner and a stronger drying effect is exerted on these trees. A further non-linear effect would be a drier, combustible litter layer in the forest floor (*Ray et al.*, 2005) that would enhance the occurrence of fires and further enhancement of tree mortality (*Cochrane et al.*, 1999). Consequently, one may conclude that interannual variability of wet season precipitation is an important characteristic of seasonality that affects stability of the rainforest system at the location of study site.

In order to further stress the latter notion, additional simulation scenarios were developed in which wet season precipitation was varied between 40% and 90%. Figure 14 illustrates the soil moisture availability factor β_T and the total recharge flux at different depths as functions of the variable wet season precipitation. As seen, the total recharge in the top 0-3 m layer scales almost linearly with reductions in wet season precipitation; a threshold effect can be observed for deeper soil layers, which are essentially not reached by the unsaturated flow if 30-50% and higher reductions are applied. Consequently, a sharp decrease in availability of

soil water is observed for overstory trees when 50% and higher reductions are used (Figure 14).

One may further hypothesize that long-term reduction of wet season precipitation can reach a threshold sufficient to cause complete mortality of overstory trees, defined by *inadequate amounts to recharge deep soils for 2-3 years in succession.* While the subsequent transient changes of the forest structure and differential responses of tree species are hard to assess, it is not impossible that the same threshold would represent a "tipping" point for the entire system, potentially leading to a collapse of the evergreen equatorial biome and its replacement by seasonal forest. This result agrees with the factors limiting the extent of evergreen forests inferred from the biogeographical study of *Hutyra et al.* (2007). This study found that forest were extant (prior to deforestation) up to a boundary where the accessible soil depth became depleted on average for two or more successive years, i.e., a very different approach lead to a similar answer to what was inferred here.

4.3 Robustness of results

The model uses a number of parameters that are reported in Tables 2 and 3. The ensemble of scenarios of soil hydraulic properties was assumed to include the possible variability of soil textures that occur in the vicinity of the flux tower site (*Hutyra et al.*, 2007). As the results demonstrate, the essential inferences of the study are not sensitive with respect to a soil hydraulic parameterization.

The parameter space of several vegetation characteristics (section 3.1) has been explored during manual model calibration efforts. However, the parameter values were kept within their narrow "biophysically-realistic" ranges that were accepted in numerous previous land-

surface modeling studies (e.g., *Bonan*, 2008). This ensures consistency with field-measured values.

The sensitivity of modeling results was explored with respect to two parameters that are particularly uncertain and hard to infer from *in situ* observations. They are the soil water potential at which stomatal closure begins, Ψ^*, and the soil water potential at which plant wilting begins, Ψ_w (Table 3). Because of the sensitivity of latent heat simulation with respect to these parameters, in all simulations they were set to sufficiently high values (i.e., low negative values). That led to a seasonally earlier onset of water stress conditions and therefore represented a less conservative approach to mimicking drought effects on the process of transpiration. For lower and higher values of these parameters, the inferences of the study remain the same, as detailed in Appendix D.

4.4 Potential applicability to other rainforest areas

One may further propose the applicability of the root niche separation hypothesis to other sites, where higher mortality of canopy-dominant trees have been observed following drought episodes. For example, *Phillips et al.* (2010) report that large trees are most vulnerable to drought-related mortality, based on an analysis of the response in forest plots to a short, intense drought in the Amazon in 2005. Yet it is hard to reconcile what appears to be a fairly high sensitivity of tree mortality reported in *Phillips et al.* (2010) study (e.g., increased mortality following a single intense drought) with an apparently more robust forest system in the Tapajós rainfall exclusion experiment, where increased mortality was not observed until the third year, which is about the same time lag necessary for reaching the drought-related "tipping point" in this modeling study. It may be difficult to draw analogies because the

754 results of *Phillips et al.* (2010) do not allow the evaluation of the circumstances under which
755 mortality occurred at different sites. Such circumstances could include the dynamics of pre-
756 2005 rainfall (e.g., consistently low annual totals could have initiated drought signal build-up
757 in deep soil before the severe 2005 episode), the increased temperatures and radiation load
758 caused by the real drought (absent from the experimental manipulation), the age charac-
759 teristics of dying trees (e.g., older trees might be more vulnerable because of imperfections
760 developed over time in xylem hydraulics that might effectively increase Ψ^* and Ψ_w), the
761 differential effects of soil textures, etc. Overall, *Phillips et al.* (2010) data neither strongly
762 confirm, nor contradict the hypothesis of root niche separation.

763 The main outcomes of the other long-term rainfall exclusion experiment in the Caxiuanã
764 National Forest in the eastern Amazon (*da Costa et al.*, 2010) were very similar to the results
765 of the experiment in Tapajós. Several hydrologically significant differences may be noted for
766 that site: (a) shallower, 10-15 m deep, sandy oxisol soils; (b) periodic wetting by groundwater
767 at 10-15 m during wet seasons, which most certainly limits the maximum rooting depth; and
768 (c) rainfall was excluded both during dry seasons and wet seasons (although *da Costa et al.*
769 (2010) note that dry seasons in Caxiuanã exhibit higher precipitation than in Tapajós). One
770 may therefore suggest that in the Caxiuanã National Forest: 1) because of a more conductive
771 soil, rainfall more rapidly recharges deeper layers, so large trees may also benefit from dry
772 season rainfall; 2) overstory trees have the opportunity to pull shallower groundwater by
773 capillarity (water table is not affected by rainfall exclusion because of flow advection in the
774 saturated zone), in the case a drought signal develops in soil; and 3) understory-medium
775 trees had somewhat less advantage, as compared to the conditions in Tapajós, because of
776 both experimentally reduced dry season rainfall and more conductive soil. This is consistent

with the observation that drought-induced mortality in the Caxiuanã experiment was not as strongly skewed towards large trees as it was in the Tapajós experiment. All of these facts are consistent with the proposed hypothesis of root niche separation. A more detailed analysis could provide more insight and a stronger possible confirmation but this is beyond the scope of the current study.

5 Conclusions

This study has addressed linkages between the subsurface moisture dynamics and evapotranspiration of a mature Amazonian rainforest. As in any modeling study, a number of simplifying assumptions were made, which are particularly difficult to avoid for such a complex system as the rainforest. Despite the fairly simple structure, the model mimics essential processes of heat flow and storage with a particular emphasis on soil hydraulics and the effects of tree root distribution on soil moisture dynamics. Specific model assumptions and relevant parameterizations are detailed in earlier work of *Ivanov et al.* (2008) and Appendices A, B, and C.

The study clearly indicates that the soil's capillary action, i.e., the upward unsaturated water flow caused by the gradient in soil matric potential due to transpirational uptake, is not a sufficient mechanism to explain stress avoidance. The estimated quantities of water transfer are too small for any permutation of soil-root scenario to justify a significant surplus of moisture available for plant uptake. The conclusion is also consistent for all soil types used in the study.

The results indicate that rainforest trees can have at least two or, most likely, a combination thereof, drought avoidance strategies at the study site. Firstly, all trees may have a *very*

deep root structure exhibiting majority of roots located in the top soil layer and progressively smaller densities at deeper locations. The open question remains though whether such deep rooting is feasible in terms of plant-soil hydraulics and soil diffusion of oxygen required for root functioning. This study has not addressed this question and detailed/mechanistic models of tree hydraulics and soil processes of gas diffusion would be needed.

The second proposed strategy is that roots of trees located at different canopy levels occupy particular water uptake niches in the soil profile. Specifically, overstory trees receive most radiation and transpire the largest amounts of water; in order to reduce the risk of vulnerability due to seasonally fluctuating rainfall, these trees developed root systems that are more uniform and extend to larger depths to exploit deeper soil moisture. During drought episodes, fractionally higher root biomass at deeper soil locations (as compared, for example, to the bulk root profile shown in Figure 3a) permits access to moisture originating from wet season precipitation. In contrast, because understory trees are constantly light-limited, their relative contribution to the total transpiration flux is significantly smaller, as compared to the contribution of overstory trees. They therefore do not need to allocate roots deeply and their root profiles contain majority of biomass in shallow surface layers. Full access to water from infrequent dry season precipitation events (and, possibly, a limited access to wet season moisture during drought periods) is sufficient for these trees to avoid seasonal drought stress. Evidence of mortaility of large overstory trees by *Nepstad et al.* (2007) at a nearby location in Tapajós and conceptually the same inference from a numerical experiment of reduction of wet season rainfall demonstrated in this study confirm that root niche separation is the likeliest the expression of the actual mechanism of drought avoidance strategy at the study location. Furthermore, a remarkable consistency of post-drought mortality of large, canopy-dominant

trees across a number of sites including Tapajós, the location of another rainfall exclusion experiment in the eastern Amazon (*da Costa et al.*, 2010), and other tropical areas (*Phillips et al.*, 2010) indicates that differential rooting depth may represent a more geographically wide-spread mechanism of adaptation of tropical trees to seasonal and interannual drought episodes. The previous biogeographical study of *Hutyra et al.* (2007) also supports the view that recharge of the deep soil reservoir every two years, or more often, is sufficient to support evergreen Amazonian forests, but forests do not survive in areas with less frequent wetting of deep soils.

Overall, the proposed adaptation strategy of root niche separation is in conceptual accordance with the likely outcome of plant trade-off between the evolutionary requirement of sustained productivity and the risks imposed by soil water limitation. By mining deep soil moisture, overstory trees exploit the buffering effect of wet season precipitation against severity of drought conditions of any particular year. As explored here in a number of synthetic scenarios, wet season rainfall therefore represents a vital characteristic affecting the stability of the rainforest system at the location of the study site.

Acknowledgments. This work supported by Ziff Postdoctoral Fellowship at the Center for the Environment at Harvard University and by the NSF grant 0911444. The technical support of the Center for Advanced Computing at the University of Michigan is acknowledged.

APPENDIX

A Model formulation details

The model formulation described in *Ivanov et al.* (2008) has been substantially modified to adapt the model to conditions of the study site. The changes are outlined in the following.

1. In order to represent the stratification of vertical canopy structure (section 2.1), the model canopy is partitioned into three layers, i.e., a "three-big-leaf" formulation of the canopy is used. The underlying idea is to represent the highest (overstory), mid-range, and smallest (understory) trees *Vieira et al.* (2004) that are parameterized as different functional types, but still classified as broadleaf evergreen tropical trees. The three-layer structure permits the resolution of the shortwave and longwave radiation distributions that drive photosynthesis, determine stomatal conductance and leaf energy balance in each "big-leaf", along with the canopy microclimate. In order to facilitate three canopy layers, the formulations of several modules have been changed.

   (a) The two-stream approximation of radiative transfer within vegetative canopies developed by *Dickinson* (1983) and *Sellers* (1985) has been analytically solved for three canopy layers. The same assumptions as specified in the original derivation were used.

   (b) The net longwave radiation for each of the canopy layers has been explicitly formulated using equations (13), (15), and (16) and the same approximation of the dependence of canopy emissivity on foliage biomass as specified in *Ivanov et al.* (2008). Note that the net longwave radiation formulated for a given canopy

layer is dependent on its canopy temperature as well as temperatures of all other layers (see Appendix B).

(c) The parameterization of admixture transfer due to forced convection has been entirely re-formulated to account for the three-layer canopy structure. Two principal transfer pathways are identified: air space above and within canopy. In the air space *above* canopy, the mean wind speed distribution follows the logarithmic profile (*Brutsaert*, 1982, p. 58) $u(z) = u_*/\kappa \ln((z - d_0)/z_{0m})$ and the turbulent (eddy) diffusivity is linear with height $K_m(z) = \kappa u_*(z - d_0)$, where z $[m]$ is the height (zero at the ground surface, positive upward), u_* $[m\ s^{-1}]$ is the friction velocity, $\kappa = 0.41$ is the von Karman constant, $H_{top} = 40.0$ $[m]$ is the assumed vegetation height at the study site, $Z_{atm} = H_{top} + 17.8$ $[m]$ is the level of wind observations, $d_0 = 29$ $[m]$ is the displacement height, and $z_{0m} = 1.3$ $[m]$ is the momentum roughness length. The two latter variables, z_{0m} and d_0, are formulated for canopy represented as a single roughness layer and their values are accepted from the study of *Simon et al.* (2005). The heat flux calculation is not sensitive to these characteristic lengths. The transfer is controlled by the bulk transfer resistance, $r_{a\,0}$ $[s\ m^{-1}]$, for the path from the top of the canopy to the level of observations obtained as

$$r_{a\,0} \;=\; \int_{H_{top}}^{Z_{atm}} K_m(z)^{-1} dz \;=\; \frac{1}{k u_*} \ln\left(\frac{Z_{atm} - d_0}{H_{top} - d_0}\right), \qquad \text{(A-1)}$$

where $u_* = u(Z_{atm})\, k \left[\ln\left(\frac{Z_{atm}-d_0}{z_{0m}}\right)\right]^{-1}$. Note that stability corrections are not explicitly introduced, which therefore assumes forced convection to be the predominant mechanism of admixture (vapor, heat) transfer. Conditions conducive

to the predominant effect of free convection and its corresponding parameterization are defined in the same fashion as specified in *Ivanov et al.* (2008).

In the air space *within* canopy, the mean in-canopy wind speed distribution is $u(z) = u(H_{top}) \exp[-a(1 - z/H_{top})]$ (*Brutsaert*, 1982, p. 100). The decrease of the eddy diffusivity K_m within canopy can be approximated with the same function (*Brutsaert*, 1982, p. 106): $K_m(z) = K_m(H_{top}) \exp[-a(1 - z/H_{top})]$, where $K_m(H_{top}) = ku_*(H_{top} - d_0)$. The parameter a is a wind decay coefficient that changes with canopy density (*Choudhury and Monteith*). In this study, it was assumed to be constant, $a = 3.0$, due to fairly small intra-annual dynamics of the canopy biomass. Subsequently, the in-canopy distribution of the bulk transfer resistance to the upward transfer of an admixture is given by $r_a(z) = \int_z^{H_{top}} K_m(x)^{-1} dx$. Note that, for any height interval within the canopy, one can define an "effective" resistance. Using the *mean* value for the bulk transfer resistance $\bar{r}_a$ $[s\, m^{-1}]$ for an i-th layer:

$$\bar{r}_{a\,i} = \frac{1}{\Delta Z} \int_{Z_{top\,i-1}}^{Z_{top\,i}} r_a(z) dz = \frac{1}{\Delta Z\, K_m(H_{top})} \left(\frac{H_{top}}{a}\right)^2 \times \left[\exp\left\{a\left(1 - \frac{Z_{top\,i-1}}{H_{top}}\right)\right\} - \exp\left\{a\left(1 - \frac{Z_{top\,i}}{H_{top}}\right)\right\}\right] - \frac{H_{top}}{a\, K_m(H_{top})} \quad \text{(A-2)}$$

where $Z_{top\,i} = H_{top}(N - i + 1)/N$ is the upper height of the i-th layer ($i = 1 \ldots 3$ for the bottom canopy layer $Z_{top\,i-1} = 0$) and $\Delta Z = Z_{top\,i} - Z_{top\,i-1}$. The total number of intervals N is assumed to be 3 in this study and therefore this formulation defines canopy layers to be uniformly distributed within the height H_{top}.

The *leaf* boundary layer resistance r_b^{leaf} (per unit leaf area), or the "excess" resistance seen by heat fluxes, varies within the canopy according to the profile of

the mean wind speed as $1/r_b^{leaf}(z) = g_b^{leaf}(z) = 0.01(u(z)/d_{leaf})^{0.5}$, where $g_b^{leaf}(z)$ is the leaf boundary layer conductance and d_{leaf} $[m]$ is the mean leaf dimension. For any given layer, the resistances act in parallel from multiple sources located at various heights z within this layer. Therefore, the *mean* resistance $\bar{r}_b$ $[s\,m^{-1}]$ for an i-th layer:

$$\frac{1}{\bar{r}_{b\,i}} = \frac{1}{\Delta Z}\int_{Z_{top\,i-1}}^{Z_{top\,i}} g_b^{leaf}(z)dz = \left(\frac{u(H_{top})}{d_{leaf}}\right)^{0.5} \frac{0.01\,H_{top}}{a\,\Delta Z} \times \left[\exp\left\{-0.5\,a\left(1-\frac{Z_{top\,i}}{H_{top}}\right)\right\} - \exp\left\{-0.5\,a\left(1-\frac{Z_{top\,i-1}}{H_{top}}\right)\right\}\right] \quad .(A\text{-}3)$$

In order to scale the leaf boundary layer resistances from the unit leaf to the unit ground area in computing heat fluxes, $\bar{r}_{b\,i}$ is multiplied by an additional factor. For sensible heat flux, the factor is $1/(\Delta L + \Delta S)$, where $\Delta L = L/3$ ($\Delta S = S/3$) is the leaf (stem) area index of the i-th layer and L is the total leaf area index (S is the total stem area index). ΔL and ΔS are assumed to be equal for all three layers because the leaf density was observed to be approximately constant throughout the canopy profile (section 2.1). For latent heat flux, the boundary layer resistance is computed separately for sunlit ("*sun*") and shaded ("*shd*") fractions of each of the canopy layers: $\bar{r}_{b\,i}^{sun} = \bar{r}_{b\,i}/L_{sun\,i}$, $r_{b\,i}^{shd} = \bar{r}_{b\,i}/L_{shd\,i}$. The total aerodynamic resistance for each of the layers is then $r_{A\,i} = r_{a\,0} + \bar{r}_{a\,i} + \bar{r}_{b\,i}$, where the last term is modified for latent heat flux according to the above presentation.

(d) The sensible and latent heat fluxes are the principal components that dissipate excess energy at each canopy level; ground heat flux is formulated as in *Ivanov et al.* (2008). Additionally, heat storage in a vegetation layer is also computed in

this study using an approximation of *Moore and Fisch* (1986). The specific heat capacity of wood, C_w, is 2.93 [$J\ g^{-1}\ K^{-1}$], the heat capacity of foliage, C_f, is 3.50 [$J\ g^{-1}\ K^{-1}$]. It is further assumed that foliage is 75% water. A time-varying canopy biomass is accounted for by specifying its annual cycle (see section 2.5.3). A constant woody biomass (including both live and dead) density is assumed to be 30 [$kg\ C\ m^{-2}$], which is higher than the total aboveground biomass estimates specified by *Nepstad et al.* (2002) and *Rice et al.* (2004) due to several reasons: to account for certain conservatism of these studies that only included trees that were larger than a certain size; and to implicitly account for the terms of biochemical energy storage and canopy air space heat storage that exhibit diurnal dynamics well correlated with the cycle of biomass heat storage (e.g., *Gu et al.*, 2007). Apparently, this indtroduces an ad-hoc assumption, however, this does not lead to a significant sensitivity in the results (tested, not shown). In fact, since the heat exchange with rain water is not simulated, the changes in the heat storage of vegetation layer maybe underestimated, especially during wet periods.

(e) Canopy Air Space (CAS) states, i.e., temperature and vapor pressure, affect the rates of sensible and latent heat fluxes (equations (26) and (28) in *Ivanov et al.* (2008)) and are defined for all canopy levels. The bottom-canopy layer CAS states are also related to the under-canopy ground temperature. See Appendix B for further details on flux computation.

(f) Energy budget is formulated for each canopy layer as well as under-canopy ground. The system of equations is composed of four equations that do not have closed forms. They are formulated implicitly, with canopy layer and ground tempera-

tures being the state unknowns. These are found by using the Newton-Raphson iteration method with most of the required derivatives approximated numerically. See Appendix B for further details on flux computation.

2. The mixed formulation of the Richards' equation (*Hillel*, 1980; *Celia et al.*, 1990) has been implemented to permit the computation of fully saturated dynamics and a proper treatment of flow in heterogeneous soils. The representation of deep soil profile explicitly resolves the propagation of wetting and drying cycles into the soil column underlying forest vegetation. This also permits the computation of capillary effects from the soil underlying the root zone.

B Energy fluxes and state variables

For a vegetated surface, the sensible and latent heat fluxes are partitioned into vegetation and ground (under-canopy) fluxes that are functions of canopy air space ("*cas*") $T_{cas,\,i}$ $[K]$, vegetation (i.e., canopy layer) $T_{v,\,i}$ $[K]$, and ground T_g $[K]$ temperatures. It is assumed that the canopy air space of a given canopy layer is not shared with other canopy layers. The canopy air space of the lowest layer, however, is affected by the energy fluxes from the underlying ground (see below).

The sensible heat flux, $H = \sum_i H_{v,\,i} + H_g$, between canopy and the atmosphere at height z_{atm} is partitioned into vegetation $H_{v,\,i}$ and ground H_g $[W\ m^{-2}]$ fluxes:

$$H_{v,\,i} = -\rho_{atm} C_p \frac{(T_{cas,\,i} - T_{v,\,i})}{r_{A,\,i}}\,, \tag{B-1}$$

$$H_g = -\rho_{atm} C_p \frac{(T_{cas,\,3} - T_g)}{r_{A,\,g}}\,, \tag{B-2}$$

where ρ_{atm} $[kg\ m^{-3}]$ is the density of moist air, $C_p = 1013$ $[J\ kg^{-1}\ K^{-1}]$ is the air heat capacity, $T_{cas,\,i}$ $[K]$ is the canopy air space temperature at level $i = 1, \ldots 3$, $r_{A,\,i}$ and $r_{A,\,g}$ $[s\ m^{-1}]$ are the bulk resistances to sensible heat flux between the vegetation/ground surface and the atmosphere.

The latent heat flux, $\lambda E = \sum_i \lambda E_{v,\,i} + \lambda E_g$, between canopy and the atmosphere at height z_{atm} is partitioned into vegetation $\lambda E_{v,\,i}$ and ground λE_g $[W\ m^{-2}]$ fluxes:

$$\lambda E_{v,\,i} = -\frac{\rho_{atm} C_p}{\gamma} \frac{(e_{cas,\,i} - e^*(T_{v,\,i}))}{r_{A,\,i}}\,, \tag{B-3}$$

$$\lambda E_g = -\frac{\rho_{atm} C_p}{\gamma} \frac{(e_{cas,\,3} - e^*(T_g)\, h_{soil})}{r_{A,\,g}}\,, \tag{B-4}$$

where λ $[J\ kg^{-1}]$ is the latent heat of vaporization, γ $[mb\ K^{-1}]$ is the psychrometric constant, $e_{cas,\,i}$ $[mb]$ is the canopy space vapor pressure at level $i = 1, \ldots 3$, $r_{A\,i}$ and $r_{A,\,g}$ $[s\ m^{-1}]$ are the bulk resistances to latent heat flux between the vegetation or ground surface and the atmosphere due to the transfer mechanisms involved (see discussion below). The term h_{soil} $[-]$ is the relative humidity of the soil pore space as in *Ivanov et al.* (2008) (eq. 20, 21).

The estimation of fluxes and temperatures for vegetated surfaces is complex because of a) the relative dependence of vegetation and ground temperatures through longwave flux; b) the highly non-linear stomatal response to change in vegetation temperature and the dependence of the latter on microclimatic conditions of canopy air space; and c) because stomatal function of temperature does not have a closed form and so does not its derivative. The canopy and ground surface energy budgets thus constitute a system of equations, which are non-linear, non-closed form functions of $T_{v,\,i}$ and T_g:

$$F_{v,\,i=1,\,2}(\mathbf{T_v}, T_g) = -\vec{S}_{v,\,i} + \vec{L}_{v,\,i}(\mathbf{T_v},\, T_g) + H_{v,\,i}(T_{v,\,i}) + \lambda E_{v,\,i}(T_{v,\,i}) + B_{v,\,i}(T_{v,\,i})\,, \tag{B-5}$$

$$F_{v,\,i=3}(\mathbf{T_v}, T_g) = -\vec{S}_{v,\,i} + \vec{L}_{v,\,i}(\mathbf{T_v},\, T_g) + H_{v,\,i}(T_{v,\,i}, T_g) + \lambda E_{v,\,i}(T_{v,\,i}, T_g) + B_{v,\,i}(T_{v,\,i}), \quad \text{(B-6)}$$

$$F_g(\mathbf{T_v}, T_g) = -\vec{S}_g + \vec{L}_g(\mathbf{T_v},\, T_g) + H_g(T_{v,\,3}, T_g) + \lambda E_g(T_{v,\,3}, T_g) + G(T_g)\,, \quad \text{(B-7)}$$

where $i = 1 \ldots 3$, $\mathbf{T_v} = [T_{v,\,1},\, \ldots\, T_{v,\,3}\,]$, B_v $[W\ m^{-2}]$ is biomass heat storage (see Appendix A), $\vec{S}$ and $\vec{L}$ $[W\ m^{-2}]$ are the net shortwave and longwave fluxes absorbed by vegetation ("v") and ground ("g"), and G $[W\ m^{-2}]$ is the ground heat flux (*Ivanov et al.*, 2008).

The Newton-Raphson iteration method is used to simultaneously solve for $T_{v,\,i}$ and T_g that balance the canopy and ground surface energy budgets. A set of linear equations for the temperature corrections $\delta\mathbf{T}$ that move functions of (B-5) through (B-7) closer to the solution can be written in the vector form as $\mathbf{J}\,\delta T = -\mathbf{F}$, where $\mathbf{F} = [F_{v,\,1},\, \ldots\, F_{v,\,3},\, F_g,\,]$, $\delta\mathbf{T} = [\Delta T_{v,\,1},\, \ldots\, \Delta T_{v,\,3},\, \Delta T_g]$, and $\mathbf{J}$ is the Jacobian matrix:

$$\mathbf{J} = \begin{bmatrix} \frac{\partial F_1}{\partial T_{v,\,1}} & \cdots & \frac{\partial F_1}{\partial T_g} \\ \cdots & \cdots & \cdots \\ \frac{\partial F_g}{\partial T_{v,\,1}} & \cdots & \frac{\partial F_g}{\partial T_g} \end{bmatrix}, \quad \text{(B-8)}$$

and

$$\begin{aligned}
\frac{\partial F_{v,\,i}}{\partial T_{v,\,i}} &= \frac{\partial \vec{L}_{v,\,i}(\mathbf{T_v},\, T_g)}{\partial T_{v,\,i}} + \frac{\partial H_{v,\,i}(T_{v,\,i})}{\partial T_{v,\,i}} + \frac{\partial \lambda E_{v,\,i}(T_{v,\,i})}{\partial T_{v,\,i}} + \frac{\partial B_{v,\,i}(T_{v,\,i})}{\partial T_{v,\,i}}\,, \\
\frac{\partial F_{v,\,i}}{\partial T_{v,\,j}} &= \frac{\partial \vec{L}_{v,\,i}(\mathbf{T_v},\, T_g)}{\partial T_{v,\,j}}\,, \\
\frac{\partial F_g}{\partial T_{v,\,i}} &= \frac{\partial \vec{L}_g(\mathbf{T_v},\, T_g)}{\partial T_{v,\,i}} + \eta\,, \\
\frac{\partial F_g}{\partial T_g} &= \frac{\partial \vec{L}_g(\mathbf{T_v},\, T_g)}{\partial T_g} + \frac{\partial H_g(T_{v,\,3}, T_g)}{\partial T_g} + \frac{\partial \lambda E_g(T_{v,\,3}, T_g)}{\partial T_g} + \frac{\partial G(T_g)}{\partial T_g}\,,
\end{aligned}$$

where $i = 1, \ldots 3$, $j = 1, \ldots 3$, $i \neq j$ and

$$\eta = 0, \quad \text{if} \quad i = 1,\ 2 \tag{B-9}$$

$$\eta = \frac{\partial H_g(T_{v,3}, T_g)}{\partial T_{v,3}} + \frac{\partial \lambda E_g(T_{v,3}, T_g)}{\partial T_{v,3}}, \quad \text{if} \quad i = 3. \tag{B-10}$$

Note that $\frac{\partial \lambda E_{v,i}(T_{v,i})}{\partial T_{v,i}}$ includes a numerical evaluation of the derivative of stomatal resistance function with respect to canopy temperature $T_{v,i}$.

C Soil moisture availability factor

A heuristic soil moisture availability factor β_T $[-]$ is used to regulate the stomatal conductance based on the soil moisture distribution in the root zone. The formulation is based on a widely used relationship (*Bonan*, 1996; *Feddes et al.*, 2001):

$$\beta_T = \sum_{j}^{N_{root}} \beta_{T,j}(z_j)\ r_j(z_j)\,, \tag{C-1}$$

$$\beta_{T,j}(z_j) = \max\left[0,\ \min\left(1,\ \frac{\theta_i(z_j) - \theta_w}{\theta^* - \theta_w}\right)\right], \tag{C-2}$$

where index j, $j = 1 \ldots N_{root}$ refers to a depth z_j $[m]$ (zero at the ground surface, positive downward) of the soil profile mesh; the root biomass fraction $r_j(z_j)$ $[-]$ is estimated such that $\sum_j^{N_{root}} r_j = 1.0$; $\theta(z_j)$ $[mm^3\ mm^{-3}]$ is the volumetric soil moisture content; θ_w $[mm^3\ mm^{-3}]$ is moisture content corresponding to the water potential Ψ_w $[MPa]$ at which plant wilting begins (Table 3); and θ^* $[mm^3\ mm^{-3}]$ is the threshold moisture content corresponding to the water potential Ψ^* $[MPa]$ at which stomatal closure begins (Table 3). Note that θ_w and θ^* depend on the selected soil water retention parameters (Table 2), following the model of

van Genuchten (1980).

Factors $\beta_{T,\,j}(z_j)$ are computed at each time step for each individual $i-$th tree type. Through their effect on the stomatal conductance (*Ivanov et al.*, 2008) they thus affect the estimation of latent heat flux $\lambda E_{v,\,i}$ in (B-3). Subsequently, factors $\beta_{T,\,j}(z_j)$ are used as weights for specifying the moisture sinks associated with transpiration in the model of soil water dynamics. Note that $\beta_{T,\,j}(z_j)$ depends on the soil hydraulic parameterization, the root profile, and the soil water distribution with depth.

From (C-1), the lumped factor $\beta_T \in [0,\ 1]$ explicitly accounts for soil moisture variability within the root profile by using appropriate weights of root biomass $r_j(z_j)$. The departure of β_T from unity indicates soil control on the transpiration flux and water limitation; $(1 - \beta_T)$ can thus be interpreted as a metric of water stress experienced by vegetation.

D Sensitivity of soil moisture availability factor

The sensitivity of modeling results was explored with respect to two parameters: the soil water potential at which stomatal closure begins, Ψ^*, and the soil water potential at which plant wilting begins, Ψ_w (Table 3). Few studies provide an indirect guidance to the possible ranges of Ψ^* and Ψ_w in a tropical rainforest (e.g., *Fisher et al.*, 2006). The parameters are uncertain and hard to interpret from *in situ* observations. It is expected that the two parameters are correlated and that their values vary among different species. Overal, for tropical species, it is likely that $\Psi^* > -1.0 - 1.5\ [MPa]$ and $\Psi_w > -3.0 - 3.5\ [MPa]$. Five additional parameter pairs of Ψ^* and Ψ_w were developed (Table 1), so as to span the range from the unlikely high values (scenario #1) to the unlikely low values (scenario #2).

In order to address the main conclusion of this study, i.e., the existence of root niches for

Table 1: The scenarios of water uptake parameters.

Parameter scenario	Ψ^*[MPa]	Ψ_w[MPa]
#1	-0.3	1.5
#2 [a]	**-0.5**	**-2.5**
#3	-0.7	-3.0
#4	-0.9	-3.3
#5	-1.1	-3.7
#6	-1.3	-4.1

[a] The scenario used in the simulations described in the main text of the manuscript (see Table 3).

trees located at different canopy levels (section 4.1), the sensitivity of results was additionally explored with respect to a hypothetical reduction in wet season precipitation. The fraction of wet season rainfall (i.e., January through June of each year) was varied between 0.4 and 1.0. The results discussed in the following correspond to two contrasting cases in which either the identical root profile was used for all tree types (the "control" root scenario #1, Figure D-1) or specific root niches were assumed (the root scenario #13, Figure D-2). The results are explored in terms of the time-averaged soil moisture availability factor β_T. The focus is on dry season periods, when water limitation may occur.

As Figure D-1 and D-2 show, the simulation results are fairly insensitive to the variation in the water uptake parameters: as the parameter values are changed according to the scenario number (x-axis in all plots), there is little effect on β_T (averaged over dry seasons) for both root scenarios. Since the factor β_T is used to constrain evapotranspiration, the same conclusion can be made with respect to the fluxes of water.

The sensitivity of β_T with respect to the wet season rainfall is clearly appreciable in Figure D-1. As the rainfall is varied from from 100% to 40% (the latter was used in the field experiment of *Nepstad et al.*, 2007), β_T becomes increasingly smaller for all tree types. A threshold for an abrupt decrease occurs at $\sim 50\%$ and further reductions are sufficient for

trees to become stressed over the long-term. If trees corresponding to different canopy levels had the same root distributions, this would result in increased mortality of all trees.

Such a sensitivity also confirms the statement of the root niche separation as the likeliest adaptation strategy. Evidently, the case with the same root profile for all tree types exhibits non-negligible water limitations even with 100% wet season rainfall (Figure D-1); as the fraction of rainfall is decreased, mid-canopy and understory trees are stressed as much as overstory trees. This is in contrast to the scenario where root profiles exhibit most differences (the root scenario #13): the root profiles of mid-canopy and understory trees exploit shallower soil moisture, while the moisture uptake profile of overtstory trees is distributed with depth more evenly. As seen in Figure D-2, overstory trees are the only ones experiencing water limitations as wet season rainfall decreases. It appears that a threshold of $\sim 45-50\%$ reduction would be sufficient for overstory trees to become stressed over the long-term, which may lead to complete mortality.

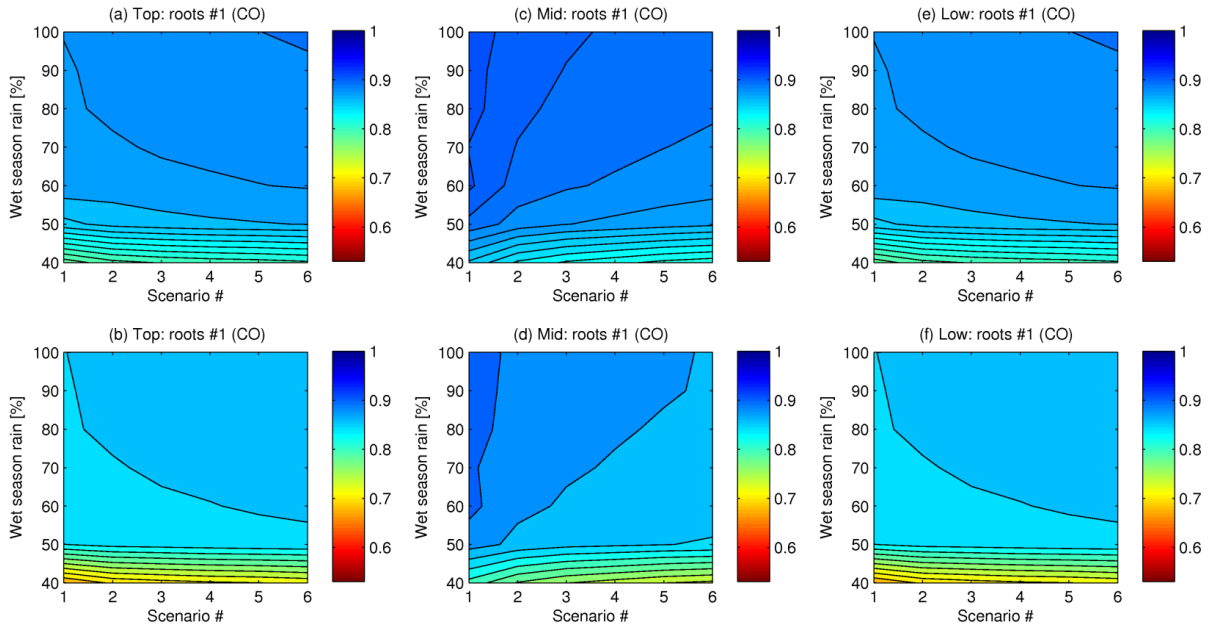

Figure D-1: The sensitivity of the soil moisture availability factor β_T to a reduction in wet season precipitation (y-axis) and water uptake parameters Ψ^* and Ψ_w (x-axis shows a scenario number). The "CO" soil type was used. Simulation results for the root scenario #1 (the same profile is used for all trees) corresponding to the maximum root depth $Z_{RootS} = 6$ m are illustrated. The averaging is carried for dry seasons only (July through December) over the periods of either 07/2002-12/2005 (subplots (a), (c), and (e)) or 07/2005-12/2005 (subplots (b), (d), and (f)). The latter period is the last year of simulation when the effect of rainfall reduction is expected to be most exacerbated.

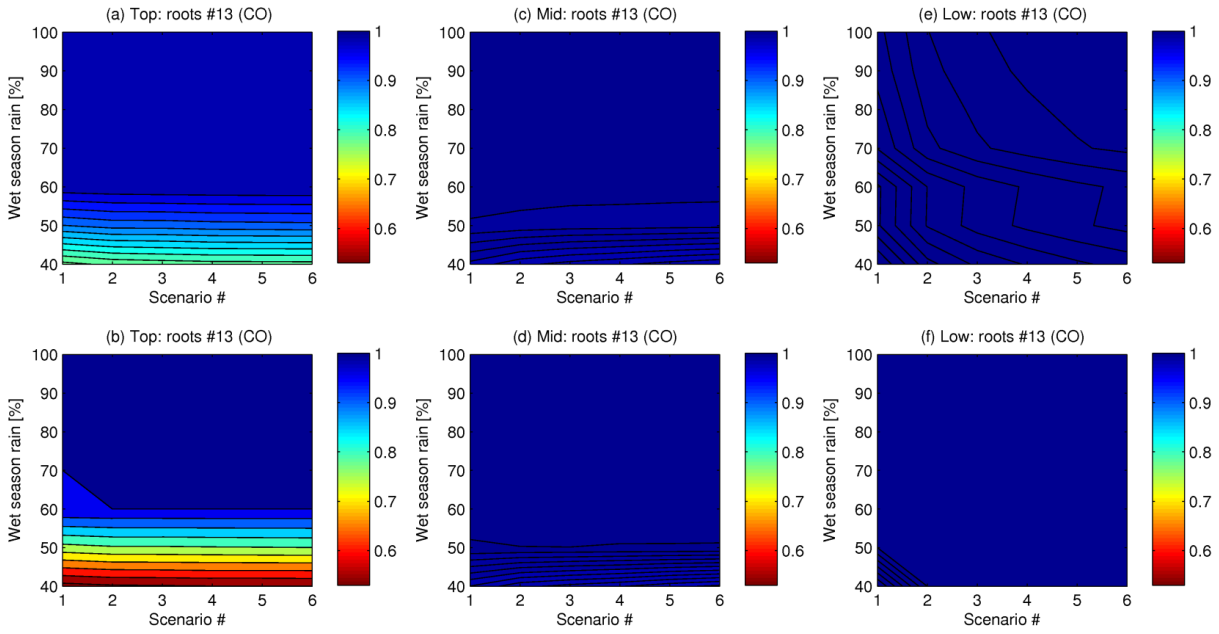

Figure D-2: The sensitivity of the soil moisture availability factor β_T to a reduction in wet season precipitation (y-axis) and water uptake parameters Ψ^* and Ψ_w (x-axis shows a scenario number). The "CO" soil type was used. Simulation results for the root scenario #13 (most different profiles) corresponding to the maximum root depth $Z_{RootS} = 6\ m$ are illustrated. The averaging is carried for dry seasons only (July through December) over the periods of either 07/2002-12/2005 (subplots (a), (c), and (e)) or 07/2005-12/2005 (subplots (b), (d), and (f)). The latter period is the last year of simulation when the effect of rainfall reduction is expected to be most exacerbated.

References

Belk, E., D. Markewitz, T. Rassmussen, E. Carvalho, D. Nepstad, and E. Davidson (2007), Modelling the effects of throughfall reduction on soil water content in a brazilian oxisol under a moist tropical forest, *Water Resources Research*, *43*(14).

Bohrer, G., G. G. Katul, R. L. Walko, and R. Avissar (2009), Exploring the effects of microscale structural heterogeneity of forest canopies using large-eddy simulations, *Boundary-Layer Meteorology*, *132*, 351–382, doi:10.1007/s10546-009-9404-4.

Bonan, G. (1996), A land surface model (lsm version 1.0) for ecological, hydrological, and atmospheric studies: technical description and user's guide, *Technical Note TN-417*, NCAR, NCAR, Boulder, CO, USA.

Bonan, G. (2008), *Ecological Climatology: Concepts and Applications*, 2nd ed., Cambridge University Press, Cambridge, UK, 568 pp.

Brando, P., D. Nepstad, E. Davidson, S. Trumbore, D. Ray, and P. Camargo (2008), Drought effects on litterfall, wood production and belowground carbon cycling in an amazon forest: results of a throughfall reduction experiment, *Philosophical Transactions of the Royal Society B*, *363*, 1839–1848.

Brando, P., S. G. A. Baccini, D. Nepstad, P. Beck, and M. C. Christman (2010), Seasonal and interannual variability of climate and vegetation indices across the amazon, *Proceedings of the National Academy of Sciences USA*, *107*(33), 14,685–14,690.

Bruno, R., H. D. Rocha, H. D. Freitas, M. Goulden, and S. Miller (2006), Soil moisture dynamics in an eastern amazonian tropical forest, *Hydrological Processes*, *20*, 2477–2489.

1077 Brutsaert, W. (1982), *Evaporation in the atmosphere. Theory, history, and applications.*, D.
1078 Reidel, Higham, MT, USA, 299 pp.

1079 Caldwell, M., T. Dawson, and J. Richards (1998), Hydraulic lift: consequences of water
1080 efflux from the roots of plants, *Oecologia*, *113*, 151–161.

1081 Cardinot, R. (2008), Efeito de seca experimental sobre a transpiração de uma floresta no
1082 centro-leste amazônico, Ph.D. thesis, University of Sao Paulo, Brasil.

1083 Celia, M., E. Bouloutas, and R. Zarba (1990), A general mass-conservative numerical solution
1084 for the unsaturated flow equation, *Water Resources Research*, *26*(7), 1483–1496.

1085 Choudhury, B., and J. Monteith (), A 4-layer model for the heat-budget of homogeneous
1086 land surfaces, *Quarterly Journal of the Royal Meteorological Society*, *114*(480), 373–398.

1087 Cochrane, M., A. Alencar, M. D. Schulze, C. Souza, and D. Nepstad (1999), Positive feed-
1088 backs in the fire dynamic of closed canopy tropical forests, *Science*, *284*, 1832–1835.

1089 Collatz, G., J. Ball, C. Grivet, and J. Berry (1991), Physiological and environmental regu-
1090 lation of stomatal conductance, photosynthesis and transpiration - a model that includes
1091 a laminar boundary-layer, *Agricultural and Forest Meteorology*, *52*(2-4), 107–136.

1092 da Costa, A. C. L., D. Galbraith, S. Almeida, B. T. T. Portela, M. da Costa, J. D. Silva,
1093 A. P. Braga, P. H. L. de Goncalves, A. A. R. de Oliveira, R. Fisher, O. L. Phillips, D. B.
1094 Metcalfe, P. Levy, and P. Meir (2010), Effect of 7 yr of experimental drought on vegetation
1095 dynamics and biomass storage of an eastern amazonian rainforest, *New Phytologist*, *187*(3),
1096 579–591.

1097 da Rocha, H., M. Goulden, S. Miller, M. Menton, L. Pinto, H. de Freitas, and A. Figueira
1098 (2004), Seasonality of water and heat fluxes over a tropical forest in eastern amazonia,
1099 *Ecological Application*, *14*(4), S22–S32.

1100 Dickinson, R. (1983), Land surface processes and climate surface albedos and energy balance,
1101 *Advances in Geophysics*, *25*, 305–353.

1102 Domingues, T., J. Berry, L. Martinelli, J. Ometto, and J. Ehleringer (2005), Parameterization
1103 of canopy structure and leaf-level gas exchange for an eastern amazonian tropical rain forest
1104 (tapajós national forest, para, brazil), *Earth Interactions*, *9*(17).

1105 Fan, Y., and G. Miguez-Macho (2010), Potential groundwater contribution to amazon dry-
1106 season evapotransporiration, *Hydrology and Earth System Sciences*, *14*, 2039–2056, doi:
1107 10.5194/hess-14-2039-2010.

1108 Farquhar, G., S. von Caemmerer, and J. Berry (1980), A biochemical model of photosynthetic
1109 CO_2 assimilation in leaves of C-3 species, *Planta*, *149*(1), 78–90.

1110 Fatichi, S., V. Y. Ivanov, and E. Caporali (2011), Simulation of future climate scenarios with
1111 a weather generator, *Advances in Water Resources*, doi:10.1016/j.advwatres.2010.12.013.

1112 Feddes, R. A., H. Hoff, M. Bruen, T. Dawson, P. de Rosnay, P. Dirmeyer, R. B. Jackson,
1113 P. Kabat, A. Kleidon, A. Lilly, and A. J. Pitmank (2001), Modeling root water uptake in
1114 hydrological and climate models, *Bulletin of the American Meteorological Society*, *82*(12),
1115 2797–2809.

1116 Fisher, R., M. Williams, R. D. Vale, A. D. Costa, and P. Meir (2006), Evidence from

amazonian forests is consistent with isohydric control of leaf water potential, *Plant, Cell and Environment*, *29*, 151–165.

Fitzjarrald, D., R. Sakai, O. Moraes, R. Oliveira, O. Acevedo, M. Czikowsky, and T. Beldini (2008), Spatial and temporal rainfall variability near the amazon tapajós confluence, *Journal of Geophysical Research*, *113*, G00B11 10.1029/2007JG000,596.

Goulden, M., S. Miller, H. da Rocha, M. Menton, H. Freitas, A. Figueira, and A. de Sousa (2004), Diel and seasonal patterns of tropical forest co_2 exchange, *Ecological Aplications*, *14*(4), S43–S54.

Grant, R., L. Hutyra, R. D. Oliveira, J. Munger, S. Saleska, and S. Wofsy (2009), Modeling the carbon balance of amazonian rain forests: resolving ecological controls on net ecosystem productivity, *Ecological Monographs*, *79*, 445–463.

Gu, L., T. Meyers, S. Pallardy, P. Hanson, B. Yang, M. Heuer, K. Hosman, Q. Liu, J. Riggs, D. Sluss, and S. Wullschleger (2007), Influences of biomass heat and biochemical energy storages on the land surface fluxes and radiative temperature, *Journal of Geophysical Research*, *112*, doi:10.1029/2006JD007425, art. no. D02107.

Hillel, D. (1980), *Fundamentals of soil physics*, Academic Press, New York, NY, USA, 413 pp.

Holben, B. (1998), Aeronet: A federated instrument network and data archive for aerosol characterization, *Remote Sensing of Environment*, *66*, 1–16.

Hou, Z., and Y. Rubin (2005), On minimum relative entropy concepts and prior compatibility

issues in vadose zone inverse and forward modeling, *Water Resources Research*, *41*(12), doi:10.1029/2005WR004082.

Huete, A., K. Didan, E. Shimabukuro, P. Ratana, S. Saleska, L. Hutyra, W. Yang, R. Nemani, and R. Myneni (2006), Amazon rainforests green-up with sunlight in dry season, *Geophysical Research Letters*, *33*(6), doi:10.1029/2005GL025583, art. No. L06405.

Hutyra, L., J. Munger, C. Nobre, S. Saleska, S. Vieira, and S. Wofsy (2005), Climatic variability and vegetation vulnerability in amazonia, *Geophysical Research Letters*, *32*(L24712).

Hutyra, L., J. Munger, S. Saleska, E. Gottlieb, B. Daube, A. Dunn, D. Amaral, P. de Camargo, and S. Wofsy (2007), Seasonal controls on the exchange of carbon and water in an amazonian rain forest, *Journal of Geophysical Research*, *112*, G03,008 10.1029/2006JG000,365.

Ichii, K., H. Hashimoto, M. White, C. Potter, L. Hutyra, A. Huete, R. Myneni, and R. Nemani (2007), Constraining rooting depths in tropical rainforests using satellite data and ecosystem modeling for accurate simulation of gross primary production seasonality, *Global Change Biology*, *13*, 67–77, doi:10.1111/j.1365-2486.2006.01277.x.

Ivanov, V. Y., R. L. Bras, and E. R. Vivoni (2008), Vegetation-hydrology dynamics in complex terrain of semiarid areas: 1. A mechanistic approach to modeling dynamic feedbacks, *Water Resources Research*, *44*(3), doi:10.1029/2006WR005588.

Jipp, P., D. Nepstad, D. Cassel, and C. Carvalho (1998), Deep soil moisture storage and transpiration in forests and pastures of seasonally-dry amazonia, *Climatic Change*, *39*, 395–412.

1158 Kleidon, A., and M. Heimann (1999), Deep-rooted vegetation, amazonian deforestation and
1159 climate: Results from a modelling study, *Global Ecol. Biogeogr.*, *8*(5), 397–405.

1160 Lee, J., R. Oliveira, T. Dawson, and I. Fung (2005), Root functioning modifies seasonal
1161 climate, *Proceedings of the National Academy of Sciences of the United States of America*,
1162 *102*(49), 17,576–17,581.

1163 Malhi, Y., and J. Wright (2004), Spatial patterns and recent trends in the climate of tropical
1164 rainforest regions, *Philosophical Transactions of the Royal Society of London, Series B*,
1165 *359*, 311–329.

1166 Moore, C., and G. Fisch (1986), Estimating heat storage in amazonian tropical forest, *Agri-*
1167 *cultural and Forest Meteorology*, *38*, 147–168.

1168 Myneni, R., S. Hoffman, Y. Knyazikhin, J. L. Privette, J. Glassy, Y. Tian, Y. Wang, X. Song,
1169 Y. Zhang, G. R. Smith, A. Lotsch, M. Friedl, J. T. Morisette, P. Votava, R. R. Nemani,
1170 and S. W. Running (2002), Global products of vegetation leaf area and fraction absorbed
1171 par from year one of modis data, *Remote Sensing of Environment*, *83*, 214–231.

1172 Myneni, R., Y. Yang, R. Ramakrishna, A. Huete, R. Dickinson, Y. Knyazikhin, K. Didan,
1173 R. Fu, R. N. Juórez, S. Saatchi, H. Hashimoto, K. Ichii, N. Shabanov, B. Tan, P. Ratana,
1174 J. Privette, J. Morisette, E. Vermote, D. Roy, R. Wolfe, M. Friedl, S. Running, P. Votava,
1175 N. El-Saleous, S. Devadiga, Y. Su, and V. Salomonson (2007), Large seasonal swings in
1176 leaf area of amazon rainforests, *Proceedings of the National Academy of Sciences, USA*,
1177 *104*, 4820–4823.

1178 Nemani, R., C. Keeling, H. Hashimoto, W. Jolly, S. Piper, C. Tucker, R. Myneni, and

S. Running (2003), Climate-driven increases in global terrestrial net primary production from 1982 to 1999, *Science*, *300*(5625), 1560–1563.

Nepstad, D., C. de Carvalho, E. Davidson, P. Jipp, P. Lefebvre, G. Negreiro, E. da Silva, T. Stone, S. Trumbore, and S. Vieira (1994), The role of deep roots in the hydrological and carbon cycles of amazonian forests and pastures, *Nature*, *372*, 666–669.

Nepstad, D., P. Moutinho, M. Dias-Filho, E. Davidson, G. Cardinot, D. Markewitz, R. Figueiredo, N. Vianna, J. Chambers, D. Ray, J. Guerreiros, P. Lefebvre, L. Sternberg, M. Moreira, L. Barros, F. Ishida, I. Tohlver, E. Belk, K. Kalif, and K. Schwalbe (2002), The effects of partial throughfall exclusion on canopy processes, aboveground production, and biogeochemistry of an amazon forest, *J. Geophys. Res.*, *107*(D20), 80–85, doi:10.1029/2001JD000360.

Nepstad, D., I. Tohver, D. Ray, P. Moutinho, and G. Cardinot (2007), Mortality of large trees and lianas following experimental drought in an amazon forest, *Ecology*, *88*, 2259–2269.

Neumann, R. B., M. Zwieniecki, Z. G. Cardon, and N. M. Holbrook (2010), The magnitude of hydraulic redistribution by plants: A laboratory investigation of biological and physical mechanisms, paper presented at the American Geophysical Union Fall 2010 Conference, San Francisco, Calif., 13-17 December.

Oliveira, R., T.E., D. S. Burgess, and D. Nepstad (2005), Hydraulic redistribution in three amazonian trees, *Oecologia*, *145*(3), 354–363.

Parrota, J., J. K. Francis, and R. Almeida (1995), *Trees of the Tapajós: A photographic field guide*, For. Serv., U.S. Dep. Of Agric., Puerto Rico, 371 pp.

1200 Phillips, O. L., G. van der Heijden, S. L. Lewis, G. Lopez-Gonzalez, L. Aragao, J. Lloyd,
1201 Y. Malhi, A. Monteagudo, S. Almeida, E. A. Davila, I. Amaral, S. Andelman, A. Andrade,
1202 L. Arroyo, G. Aymard, T. R. Baker, L. Blanc, D. Bonal, A. C. A. de Oliveira, K. J. Chao,
1203 N. D. Cardozo, L. da Costa, T. R. Feldpausch, J. B. Fisher, N. M. Fyllas, M. A. Freitas,
1204 D. Galbraith, E. Gloor, N. Higuchi, E. Honorio, E. Jimenez, H. Keeling, T. J. Killeen, J. C.
1205 Lovett, P. Meir, C. Mendoza, A. Morel, P. N. Vargas, S. Patino, K. S. H. Peh, A. P. Cruz,
1206 A. Prieto, C. A. Quesada, F. Ramirez, H. Ramirez, A. Rudas, R. Salamao, M. Schwarz,
1207 J. Silva, M. Silveira, J. W. F. Slik, B. Sonke, A. S. Thomas, J. Stropp, J. R. D. Taplin,
1208 R. Vasquez, and E. Vilanova (2010), Drought-mortality relationships for tropical forests,
1209 *New Phytologist*, *187*(3), 631–646.

1210 Popper, K. (1972), *Objective Knowledge: An Evolutionary Approach*, Oxford University
1211 Press, USA, revised edition (November 9, 1972), 390 pp.

1212 Ray, D., D. Nepstad, and P. Moutinho (2005), Micrometeorological and canopy controls of
1213 fire susceptibility in a forested amazon landscape, *Ecological Applications*, *14*, 1664–1678.

1214 Rice, A., E. Hammond, S. Saleska, L. Hutyra, M. Palace, M. Keller, P. de Carmargo, K. Por-
1215 tilho, D. Marques, and S. Wofsy (2004), Carbon balance and vegetation dynamics in an
1216 old-growth amazonian forest, *Ecological Applications*, *14*(4), s55–s71.

1217 Romero-Saltos, H., L. da S.L. Sternberg, M. Moreira, and D. Nepstad (2005), Ranifall exclu-
1218 sion in an eastern amazonian forest alters soil water movement and depth of water uptake,
1219 *American Journal of Botany*, *92*, 443–455.

1220 Sakai, R., D. Fitzjarrald, O. Moraes, R. Staebler, O. Acevedo, M. Czikowsky, R. D. Silva,
1221 E. Brait, and V. Miranda (2004), Land-use change effects on local energy, water, and

carbon balances in an amazonian agricultural field, *Global Change Biology*, *10*(5), 895–907.

Saleska, S., S. Miller, D. Matross, M. Goulden, S. Wofsy, H. da Rocha, P. de Camargo, P. Crill, B. Daube, H. de Freitas, L. Hutyra, M. Keller, V. Kirchhoff, M. Menton, J. Munger, E. Pyle, A. Rice, and H. Silva (2003), Carbon in amazon forests: Unexpected seasonal fluxes and disturbance-induced losses, *Science*, *302*, 1554–1557.

Saleska, S., K. Didan, A. Huete, and H. da Rocha (2007), Amazon forests green-up during 2005 drought, *Science*, *318*, 612–612.

Schenk, H., and R. Jackson (2002), The global biogeography of roots, *Ecological Monographs*, *72*, 311–328.

Schlesinger, W. (1997), *iogeochemistry: An Analysis of Global Change*, Academic Press, New York, NY, 588 pp.

Sellers, P. (1985), Canopy reflectance, photosynthesis and transpiration, *International Journal of Remote Sensing*, *6*(8), 1335–1372.

Shuttleworth, W. (1988), Evaporation from amazonian rainforests, *Proceedings of the Royal Society of London, Series B, Biological Sciences*, *233*(1272), 321–246.

Silver, W., J. Neff, M. McGroddy, E. Veldkamp, M. Keller, and R. Cosme (2000), Effects of soil texture on belowground carbon and nutrient storage in a lowland amazonian forest ecosystem, *Ecosystems*, *3*, 193–209.

Simon, E., F. Meixner, L. Ganzeveld, and J. Kesselmeier (2005), Coupled carbon-water

exchange of the amazon rain forest, i. model description, parameterization and sensitivity analysis, *Biogeosciences*, *2*, 231–253.

Sombroek, W. (2001), Spatial and temporal patterns of amazon rainfall, *Ambio*, *30*, 388–396.

Taiz, L., and E. Zeiger (2006), *Plant Physiology*, 4th ed., Sinauer Associates, Inc., MA, USA, 700 pp.

Tomasella, J., M. Hodnett, and L. Rossato (2000), Pedotransfer functions for the estimation of soil water retention in brazilian soils, *Soil Sci. Soc. Am. J.*, *64*, 327–338.

van Genuchten, M. T. (1980), A closed-form equation for predicting the hydraulic conductivity of unsaturated soils, *Soil Science Society of America Journal*, *44*, 892–898.

Vieira, S., P. de Camargo, D. Selhorst, R. da Silva, L. Hutyra, J. Chambers, I. Brown, N. Higuchi, J. dos Santos, S. Wofsy, S. Trumbore, and L. Martinelli (2004), Forest structure and carbon dynamics in amazonian tropical rain forests, *Oecologia*, *140*, 468–479.

List of Tables

3 Vegetation biophysical, photosynthesis, interception, and water uptake parameters used in the model (for details see *Ivanov et al.*, 2008): d_{leaf} $[m]$ is the mean leaf size, χ_L is the parameter of departure of leaf angles from a random distribution, α_Λ^{leaf} and τ_Λ^{leaf} $[-]$ are the leaf reflectances and transmittances, respectively, α_Λ^{stem} and τ_Λ^{stem} $[-]$ are the stem reflectances and transmittances, respectively, "VIS" and "NIR" are used to denote the visible and near-infrared spectral bands, respectively, $V_{max\,25}$ $[\mu mol\ \mathrm{CO}_2\ m^{-2}\ s^{-1}]$ is the maximum catalytic capacity of Rubisco at 25℃, $\bar{K}$ $[-]$ is the time-mean PAR extinction coefficient used to parameterize a decay of nitrogen content in the canopy, m $[-]$ is an empirical parameter used as a slope factor in a linear model relating the net assimilation rate and stomatal conductance, b $[\mu mol\ m^{-2}\ s^{-1}]$ is the minimum stomatal conductance, $\epsilon_{3,4}$ $[\mu mol\ \mathrm{CO}_2\ \mu mol^{-1}\ photons]$ is the intrinsic quantum efficiency of CO_2 uptake, K_c $[mm\ hour^{-1}]$ is the canopy water drainage rate coefficient, g_c $[mm^{-1}]$ is the exponent parameter of canopy water drainage rate, Ψ^* $[MPa]$ is the soil water potential at which stomatal closure begins, and Ψ_w $[MPa]$ is the soil water potential at which plant wilting begins. 64

Table 2: The soil hydraulic, heat transfer, and albedo parameters for different soil parameterization scenarios: $K_{s\,n}$ $[mm\ hour^{-1}]$ is the saturated hydraulic conductivity in the normal to the soil's surface direction, θ_s $[mm^3\ mm^{-3}]$ is the saturation moisture content, θ_r $[mm^3\ mm^{-3}]$ is the residual moisture content, n and α $[mm^{-1}]$ are the fit parameters of the van Genuchten-Mualem soil hydraulic model (*van Genuchten*, 1980). The soil albedo and heat transfer[a] parameters are assumed to be uniform for all soil parameterizations.

Soil scenario / Parameter	$K_{s\,n}$	θ_s	θ_r	n	α
CO - surface[b]	35.6	0.647	0.225	1.237	-0.0883
CO - deep[b]	14.1	0.578	0.291	1.413	-0.00674
TH[b]	14.1	0.696	0.315	1.687	-0.0224
MRE[b]	26.9	0.604	0.283	1.0623	-0.0213

[a] Since under-canopy soil is assumed to be a Lambertian surface, albedos for direct beam, α^{μ}_{Λ}, and diffuse, α_{Λ}, shortwave radiation fluxes are equal. The values of the shortwave albedos for *saturated* soil ($\alpha^{\mu}_{sat\,\Lambda} = \alpha_{sat\,\Lambda}$) are 0.11 for the visible and 0.225 for the near-infrared spectral bands, respectively (*Ivanov et al.*, 2008). The values of the shortwave albedos for *dry* soil ($\alpha^{\mu}_{dry\,\Lambda} = \alpha_{dry\,\Lambda}$) are 0.22 for the visible and 0.45 for the near-infrared spectral bands, respectively. The soil heat transfer properties are assigned the following values: $k_{s,\,dry} = 0.4$ and $k_{s,\,sat} = 3.3$ $[J\ m^{-1}\ s^{-1}\ K^{-1}]$ are the *dry* and *saturated* soil thermal conductivities, respectively, and $C_{s,\,soi} = 1.5 \times 10^6$ $[J\ m^{-3}\ K^{-1}]$ is the heat capacity of the soil solid (*Ivanov et al.*, 2008).

[b] See section 2.3 for the definitions of soil parameterization scenarios.

Table 3: Vegetation biophysical, photosynthesis, interception, and water uptake parameters used in the model (for details see *Ivanov et al.*, 2008): d_{leaf} $[m]$ is the mean leaf size, χ_L is the parameter of departure of leaf angles from a random distribution, α_Λ^{leaf} and τ_Λ^{leaf} $[-]$ are the leaf reflectances and transmittances, respectively, α_Λ^{stem} and τ_Λ^{stem} $[-]$ are the stem reflectances and transmittances, respectively, "VIS" and "NIR" are used to denote the visible and near-infrared spectral bands, respectively, $V_{max\,25}$ $[\mu mol\ \mathrm{CO_2}\ m^{-2}\ s^{-1}]$ is the maximum catalytic capacity of Rubisco at 25℃, $\bar{K}$ $[-]$ is the time-mean PAR extinction coefficient used to parameterize a decay of nitrogen content in the canopy, m $[-]$ is an empirical parameter used as a slope factor in a linear model relating the net assimilation rate and stomatal conductance, b $[\mu mol\ m^{-2}\ s^{-1}]$ is the minimum stomatal conductance, $\epsilon_{3,4}$ $[\mu mol\ \mathrm{CO_2}\ \mu mol^{-1}\ photons]$ is the intrinsic quantum efficiency of $\mathrm{CO_2}$ uptake, K_c $[mm\ hour^{-1}]$ is the canopy water drainage rate coefficient, g_c $[mm^{-1}]$ is the exponent parameter of canopy water drainage rate, Ψ^* $[MPa]$ is the soil water potential at which stomatal closure begins, and Ψ_w $[MPa]$ is the soil water potential at which plant wilting begins.

Parameter / Canopy level	**Top-canopy**	**Mid-canopy**	**Bottom-canopy**
Biophysical parameters			
d_{leaf}	0.05	0.05	0.05
χ_L	0.10	0.10	0.10
α_Λ^{leaf} - VIS	0.11	0.05	0.02
α_Λ^{leaf} - NIR	0.50	0.50	0.50
α_Λ^{stem} - VIS	0.20	0.20	0.20
α_Λ^{stem} - NIR	0.45	0.45	0.45
τ_Λ^{leaf} - VIS	0.07	0.02	0.01
τ_Λ^{leaf} - NIR	0.33	0.32	0.32
τ_Λ^{stem} - VIS	0.0001	0.0001	0.0001
τ_Λ^{stem} - NIR	0.0001	0.0001	0.0001
Photosynthesis parameters			
$V_{max\,25}$	40.0	35.0	30.0
$\bar{K}$	0.35	0.35	0.35
m	9	9	9
b	10,000	10,000	10,000
$\epsilon_{3,4}$	0.055	0.06	0.065
Interception parameters			
K_c	0.15	0.15	0.15
g_c	3.7	3.7	3.7
Water uptake parameters			
Ψ^*	-0.50	-0.50	-0.50
Ψ_w	-2.50	-2.50	-2.50

List of Figures

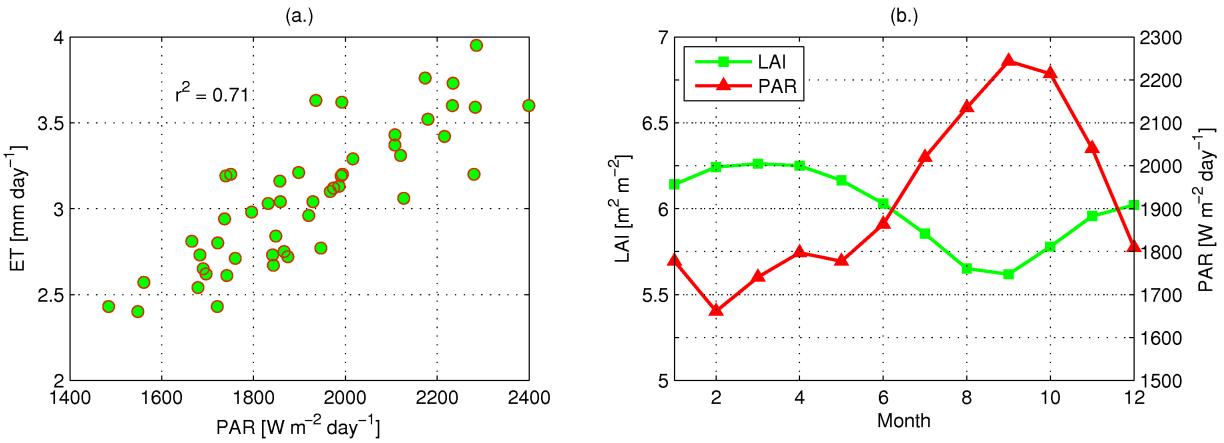

Figure 1: a) A relationship between the observed mean monthly downwelling photosynthetically active radiation (PAR) and mean monthly evapotranspiration (ET). Both fluxes are resolved as mean daily quantities. b) The mean observed annual cycles of PAR and leaf area index (LAI, the data on were obtained from the database of the Large Scale Biosphere-Atmosphere Experiment in Amazonia, *http://lba.cptec.inpe.br*). Observations of PAT and ET were obtained in the Tapajós National Forest (Brazil) near km 67 of the Santarém-Cuiabá highway and were previously described in *Hutyra et al.* (2007).

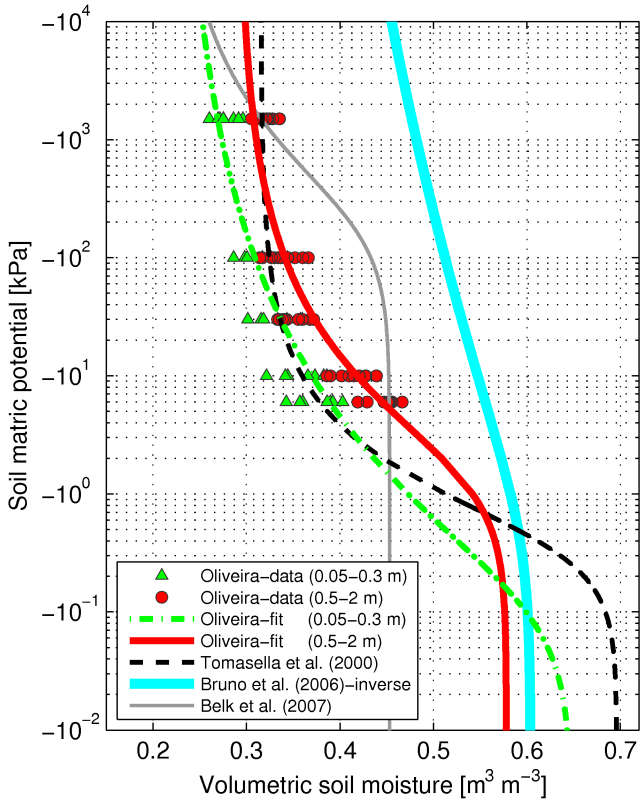

Figure 2: Soil water retention data and curves obtained in this study. The curves were parameterized according to the van Genuchten-Mualem soil hydraulic model (*van Genuchten*, 1980). The legend notation refers to the following sources: "Oliveira-data" refers to the data obtained from R. C. de Oliveira in 2007; "Oliveira-fit" refers to the fit curves obtained for the former data for different depth ranges; "Tomasella et al. (2000)" refers to parameters obtained with the pedotransfer functions of *Tomasella et al.* (2000) using field soil texture data of L. Hutyra (obtained in 2003); "Bruno et al. (2006)-inverse" refers to the parameters of soil water retention curve obtained using an inverse procedure of *Hou and Rubin* (2005); and "Belk et al. (2007)" refers to the curve obtained by geometric averaging of depth-interpolated parameters reported in *Belk et al.* (2007).

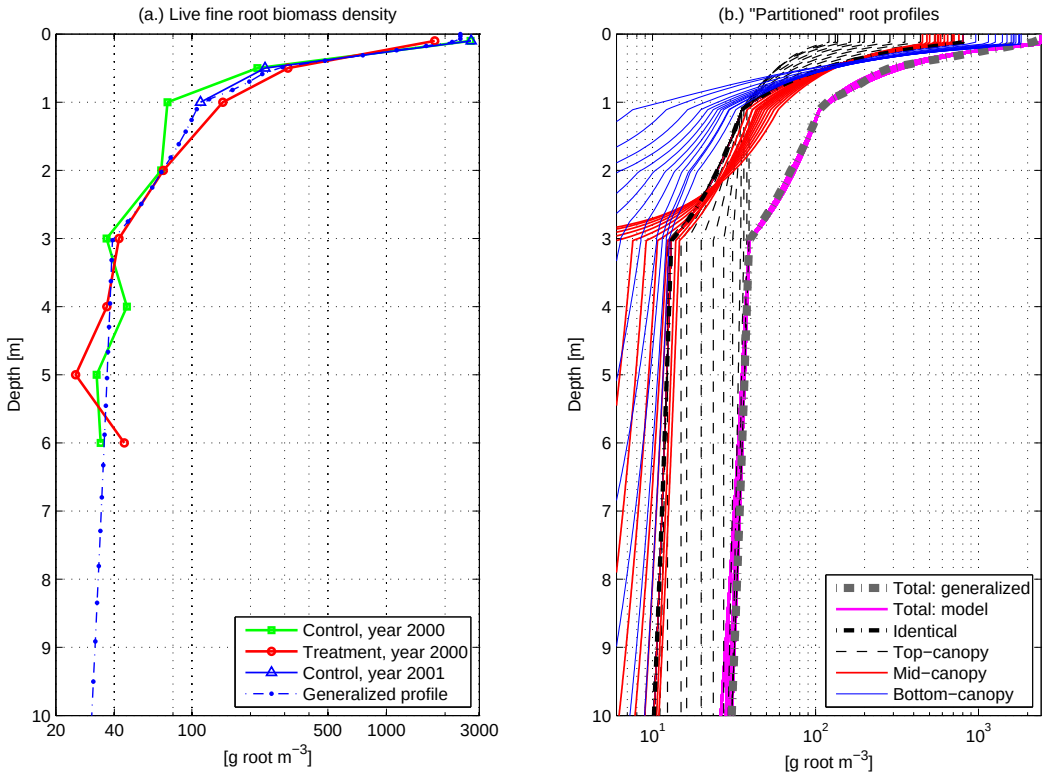

Figure 3: Profiles of root biomass distribution: a) live fine root density from *Nepstad et al.* (2002), corresponding to measurements in the "control" and "treatment" plots, and a generalized profile obtained in this study; and b.) hypothesized root profiles (section 2.5.4) obtained by partitioning the observed profile of bulk root biomass into profiles corresponding to top-, mid-, and bottom-canopy trees. In total, 13 different permutations of root profiles were generated. The "*Total: generalized*" represents the generalized profile of bulk root density shown in Figure 3a; the "*Total: model*" profiles are obtained by summing three density profiles corresponding to different trees (13 permutations). The "*Identical*" profile illustrates the root scenario #1, i.e., all tree types have the same root density profile.

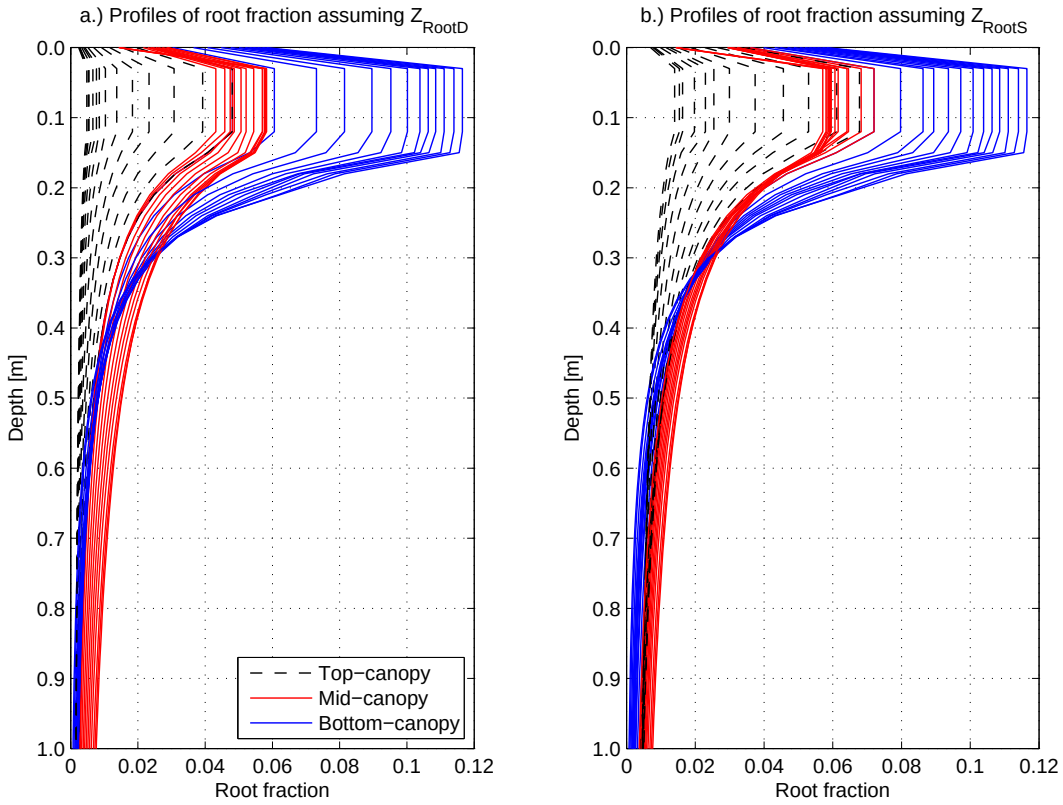

Figure 4: Root fractional distributions resulting from mapping the root profiles onto the model subsurface mesh (30 mm regular spacing). The distributions were obtained from the 13 permutations of root density profiles for trees representing different canopy levels (Figure 3): a) the profiles corresponding to the deeper maximum root depth $Z_{RootD} = 30.2$ m; and b) the profiles corresponding to the shallower maximum root depth $Z_{RootS} = 6$ m. Distributions only for the top 70 cm of soil are shown, where most pronounced differences among the profiles are observed.

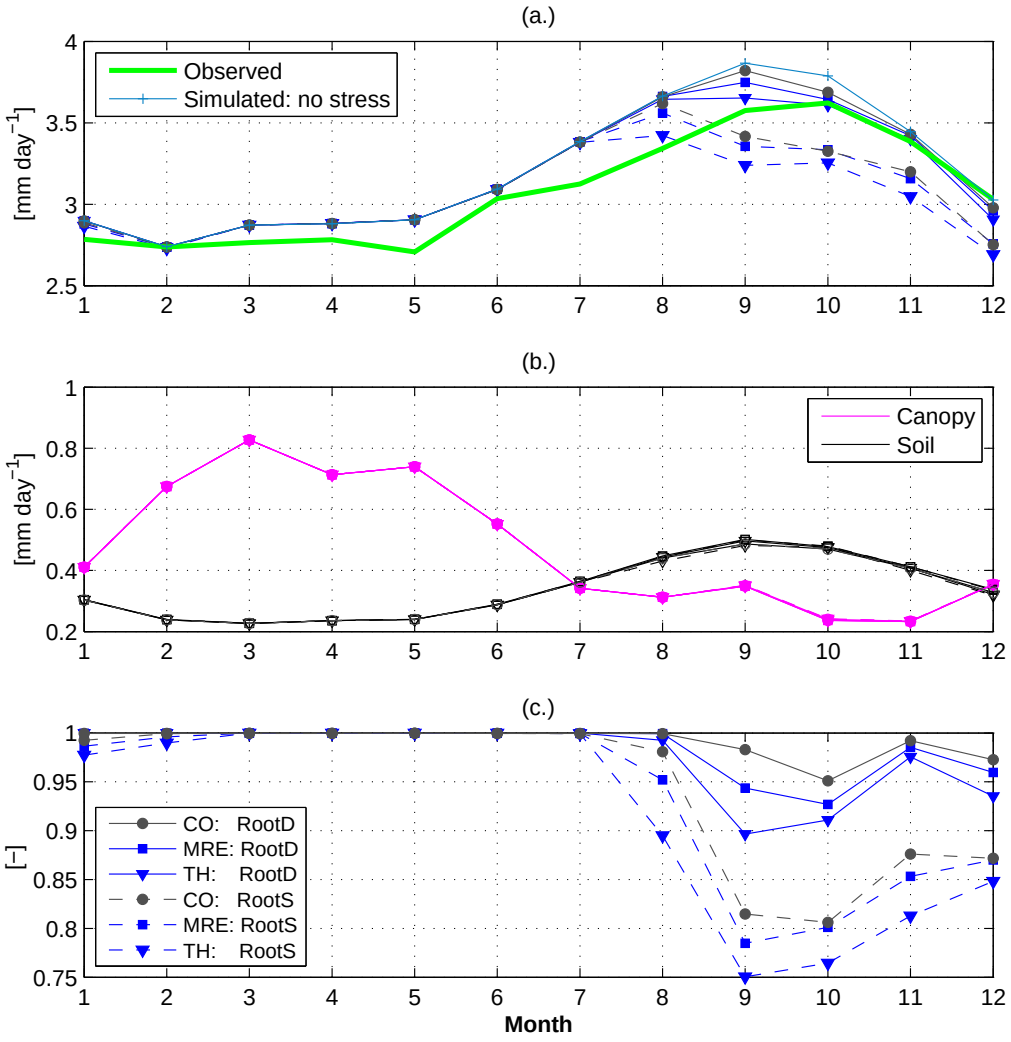

Figure 5: The mean annual cycles of a) the total evapotranspiration (observed and simulated); b) evaporation from canopy interception storage and soil surface (simulated); c) soil moisture availability factor, β_T (Appendix C, eq. (C-1)), computed as the arithmetic average for the three tree types. The annual cycles were computed for the period of 01/2002-01/2006. The "no stress" scenario (shown in subplot (a) only) corresponds to "potential evapotranspiration", a synthetic case with soil moisture stress set to zero at each computational step (section 3.1). All other scenarios correspond to simulated actual evapotranspiration and exhibit seasonal stress (subplot (c)). "RootD" corresponds to deep roots (the maximum root depth $Z_{RootD} = 30.2\ m$) and the identical root profile (the root scenario #1, Figure 3b); "RootS" corresponds to shallow roots (the maximum root depth $Z_{RootS} = 6\ m$ and the identical root profile (the root scenario #1). Results for the three soil types are illustrated: "CO", "MRE", and "TH" (Table 2).

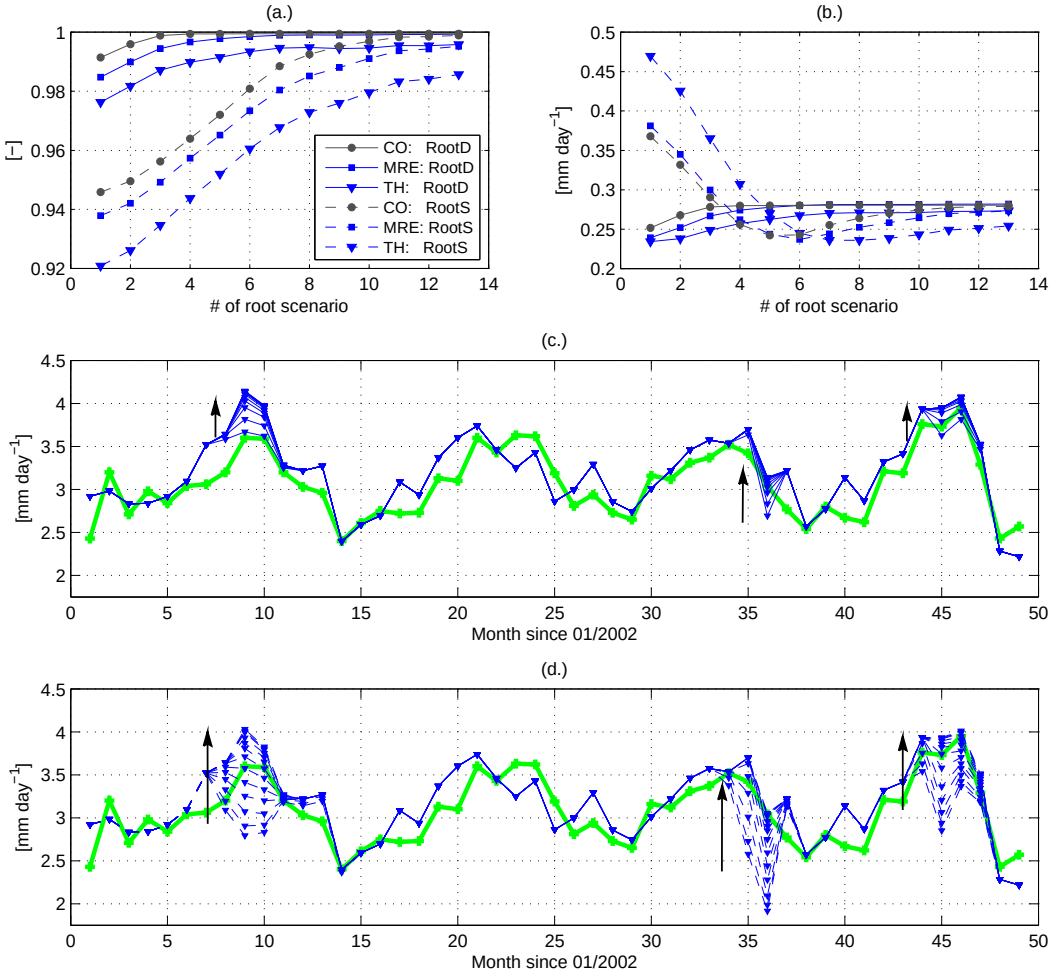

Figure 6: The results of numerical experiments for different scenarios of root distributions. a) The mean soil moisture availability factor β_T; each point corresponds to a particular permutation scenario of root distributions (section 2.5.4) and was computed as the average value for the three tree types for the simulation period of 01/2002-01/2006. b) The root mean square error of simulated mean daily evapotranspiration (resolved at the monthly scale for dry seasons only); each point corresponds to a particular permutation scenario of root distributions and represents an average value for the simulation period of 01/2002-01/2006. c) An illustration of the effect of deep root permutation scenarios (the maximum root depth is $Z_{RootD} = 30.2\ m$) on the simulation of daily evapotranspiration resolved at the monthly scale. d) Same as c) but with shallower root scenarios (the maximum root depth is $Z_{RootS} = 6\ m$). For c) and d), the arrows indicate a direction of increase of the root scenario number (from #1, the identical distribution, to #13, distinct root niches, see Figure 3b). The "TH" soil type was used.

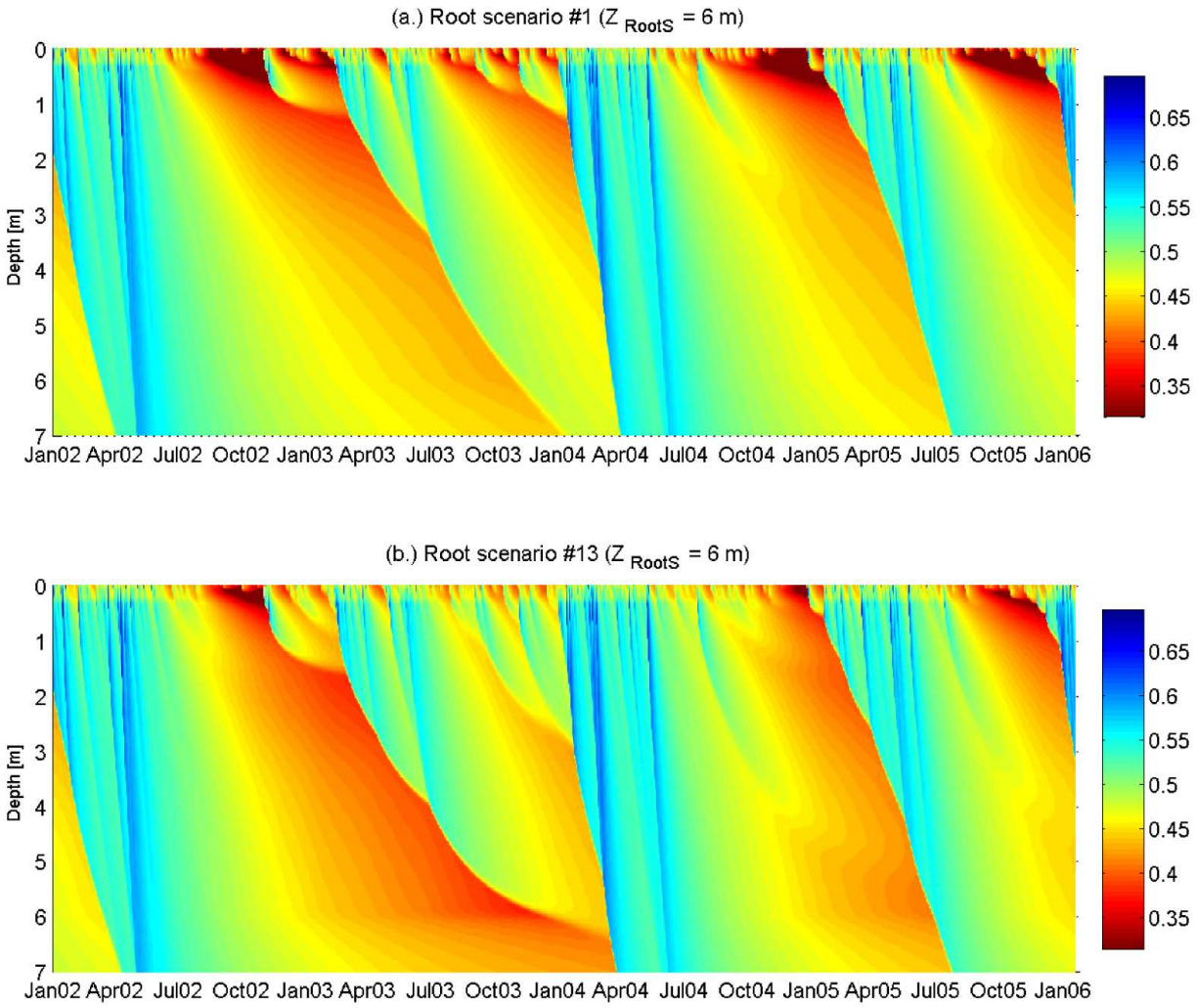

Figure 7: The temporal evolution of soil moisture profile for two root scenarios corresponding to the maximum root depth Z_{RootS}. a) Simulation results for the root scenario #1 are illustrated, which exhibits the same fractional distribution of roots for all tree types (Figure 4b, approximately corresponding to the convergence of distributions in the middle of the figure). b) Simulation results for the root scenario #13 are shown. The scenario assumes that trees of the upper canopy level contain a higher fraction of roots at deeper locations (Figure 4b, left hand-side dashed line), while trees of the bottom canopy layer contain higher fraction of roots at shallower soil layers (Figure 4b, right hand-side solid line). The "CO" soil type was used.

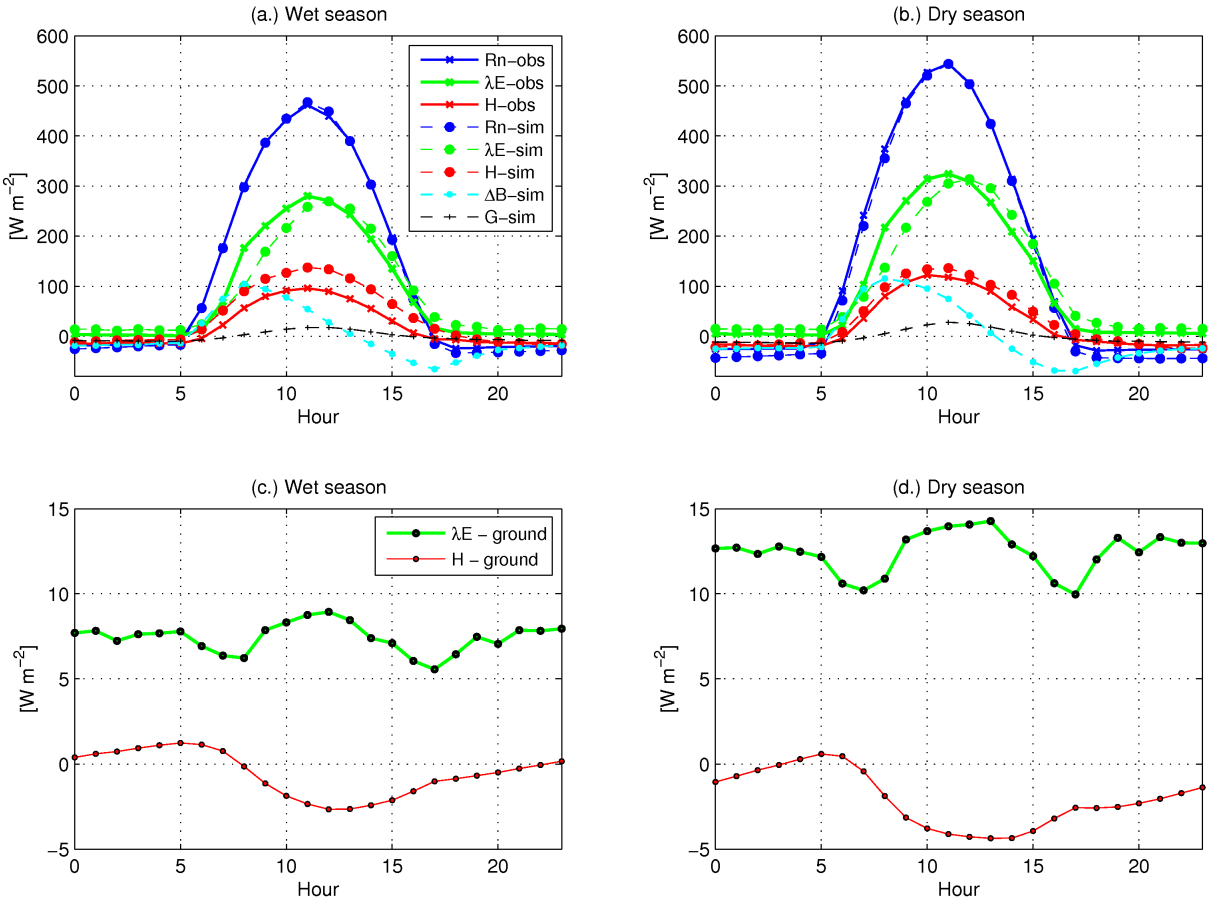

Figure 8: Mean observed and simulated diurnal cycles of energy: for wet season (defined as the period between December 16th and July 14th), subplots (a.) and (c.); and for dry season (defined as the period between July 15th and December 15th of each calendar year), subplots (b.) and (d.). Notation used: Rn is net radiation, λE is latent heat flux, H is sensible heat flux, ΔB is change in heat storage in biomass and air, G is ground heat flux; "obs" refers to measured series; "sim" refers to simulated results; "ground" refers to contribution from undercanopy ground (simulated cycles only). Simulation results of "CO" soil parameterization (root scenario #6) were used.

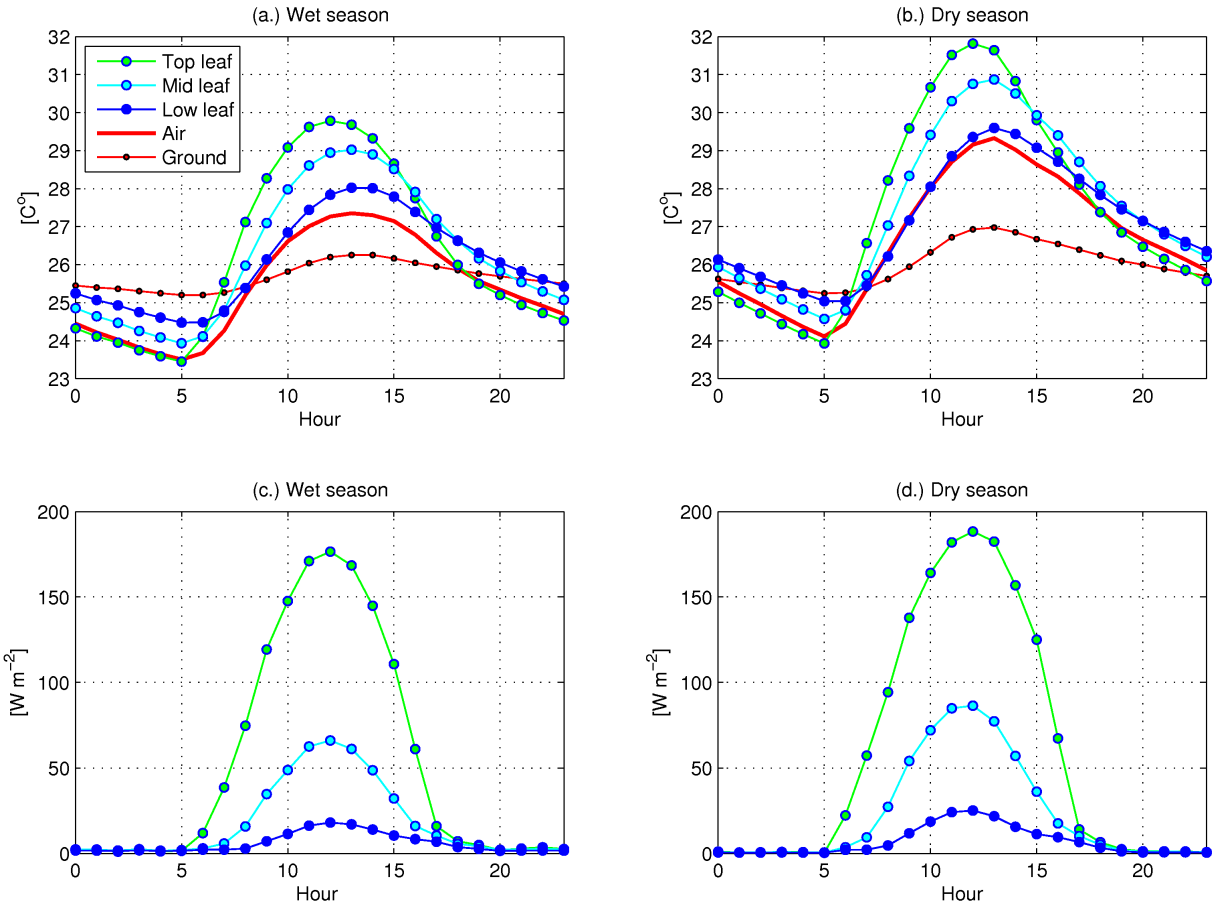

Figure 9: Mean diurnal cycles of air and canopy layer temperature and latent heat flux: for wet season (defined as the period between December 16th and July 14th), subplots (a.) and (c.); and for dry season (defined as the period between July 15th and December 15th of each calendar year), subplots (b.) and (d.). "Air" refers to measured above-canopy air temperature; "Top leaf" refers to top canopy layer; "Mid leaf" refers to middle canopy layer; "Low leaf" refers to bottom canopy layer; and "Ground" refers to undercanopy soil surface. Subplots (a.) and (b.) illustrate mean temperature cycles; subplots (c.) and (d.) show mean simulated cycles of latent heat flux. Simulation results of "CO" soil parameterization (root scenario #6) were used.

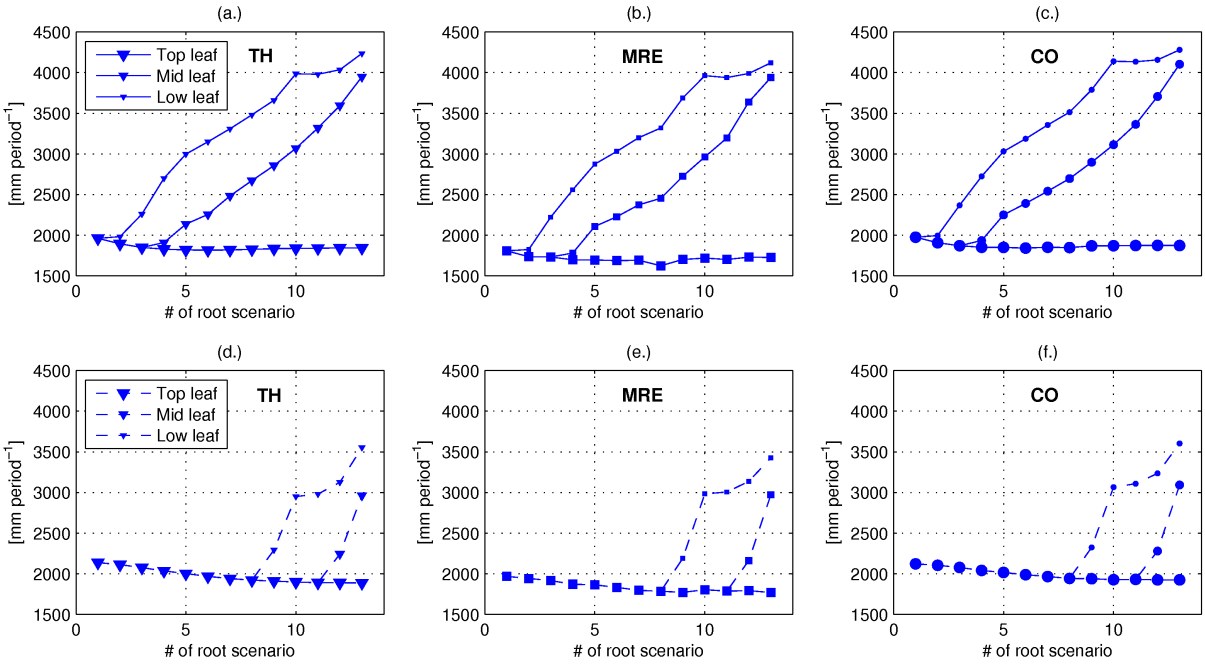

Figure 10: The integrated flux at the bottom of root zone of each tree type computed over the 01/2002-01/2006 simulation period in relation to the root scenario number. Plots (a.) through (c.): the results correspond to the maximum root depth $Z_{RootD} = 30.2\ m$; plots (d.) through (f.): the results correspond to the maximum root depth $Z_{RootS} = 6\ m$. The soil scenarios are denoted in the plots: (a.) and (d.) correspond to "TH"; (b.) and (e.) correspond to "MRE"; and (c.) and (f.) correspond to "CO". The larger symbol size denotes the higher canopy level.

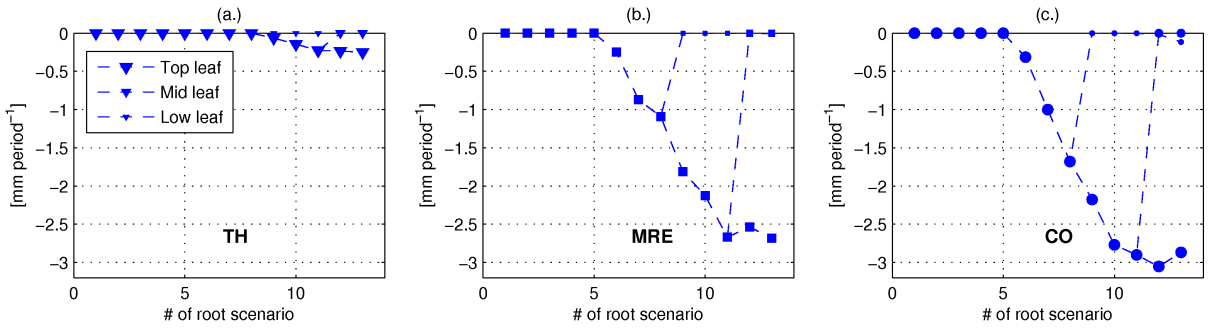

Figure 11: The integrated capillary (upward) flux into the root zone of each tree type over the 01/2002-01/2006 simulation period in relation to the root scenario number. Plots (a.) through (c.): the results correspond to the maximum root depth $Z_{RootS} = 6\ m$ (the shallower root scenarios). Soil scenarios are denoted in the plots: (a.) corresponds to "TH"; (b.) corresponds to "MRE"; and (c.) corresponds to "CO". The larger symbol size denotes the higher canopy level.

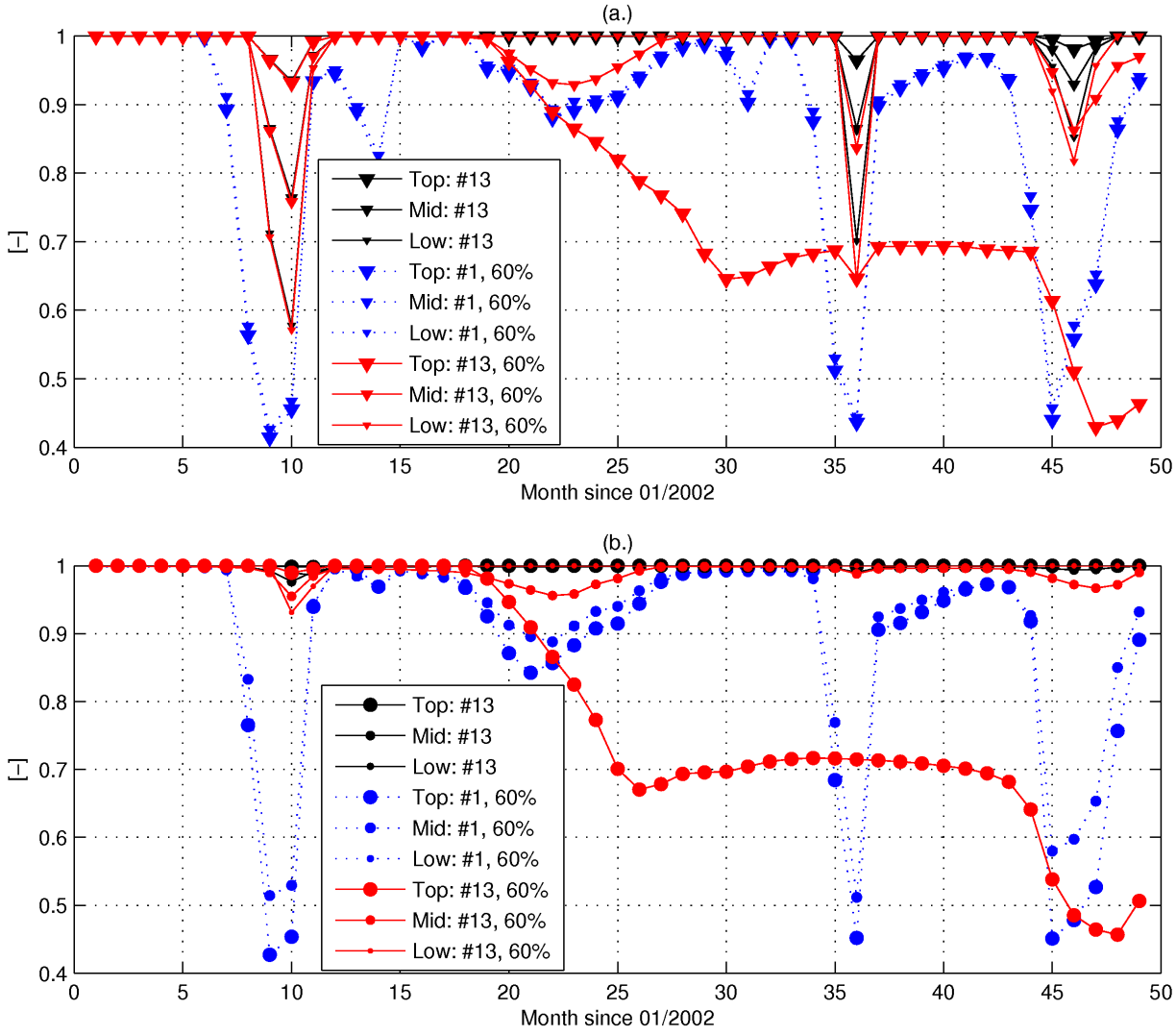

Figure 12: The time series of soil moisture availability factor β_T for each tree type: top ("Top") canopy layer, middle ("Mid") canopy layer, and bottom ("Low") level canopy over the 01/2002-01/2006 period of simulation. The subplot (a.) corresponds to the "TH" soil type; the subplot (b.) corresponds to the "CO" soil type. The maximum root depth $Z_{RootS} = 6\ m$ was used with two types of profile distributions: root scenarios #1 (the same profile is used for all trees) and #13 (most different profiles). The "60%" notation is used for the scenario in which wet season (January through June of each year) precipitation was reduced by 60%.

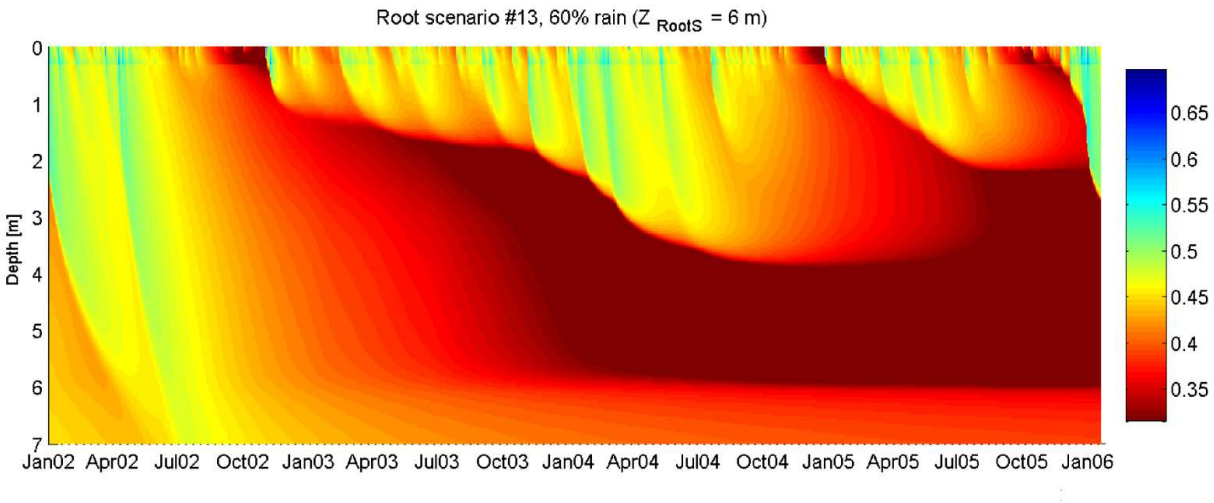

Figure 13: The temporal evolution of soil moisture profile for a scenario in which wet season (January through June of each year) precipitation was reduced by 60%. Simulation results for the root scenario #13 corresponding to the maximum root depth Z_{RootS} are illustrated. The "CO" soil type was used.

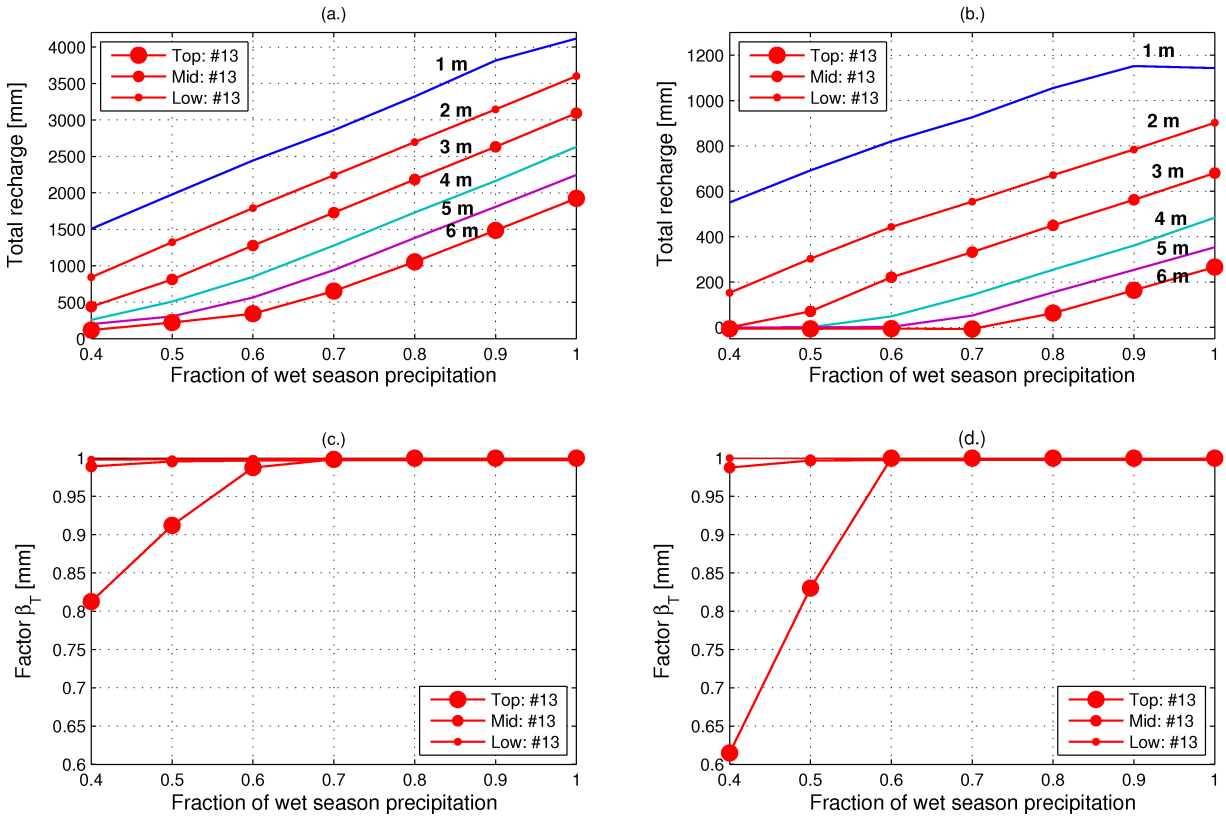

Figure 14: The sensitivity of the total recharge flux and the soil moisture availability factor β_T to a reduction in wet season (January through June of each year) precipitation. The wet season precipitation was varied between 40% and 100% (the x-axis in each subplot). Simulation results for the root scenario #13 corresponding to the maximum root depth $Z_{RootS} = 6$ m are illustrated. The "CO" soil type was used. Subplots (a) and (c) correspond to the integration over the 01/2002-01/2006 period of simulation; subplots (b) and (d) correspond to the integration over the 01/2005-01/2006 period, i.e., the last year of simulation when the effect of rainfall reduction is expected to be most exacerbated. The lines with circle symbols in (a) and (b) correspond to approximate depths of the root zone bottom for trees at different canopy levels, i.e., 2, 3, and 6 m in the root scenario #13.